NASA Technical Memorandum 84584

High-Angle-of-Attack Stability Characteristics of a Three-Surface Fighter Configuration

Sue B. Grafton, Mark A. Croom,
and Luat T. Nguyen

MARCH 1983

NASA

NASA Technical Memorandum 84584

High-Angle-of-Attack Stability Characteristics of a Three-Surface Fighter Configuration

Sue B. Grafton, Mark A. Croom,
and Luat T. Nguyen
Langley Research Center
Hampton, Virginia

NASA
National Aeronautics
and Space Administration
Scientific and Technical
Information Branch
1983

SUMMARY

A wind-tunnel investigation was conducted to study the low-speed, high-angle-of-attack stability characteristics of a three-surface fighter concept based on the F-15 configuration. Static-force data were measured over angle-of-attack and sideslip ranges of 0° to 85° and -10° to 10°, respectively. A forced-oscillation technique was used to obtain dynamic derivatives at angles of attack from 0° to 60°. The tests were conducted for several canard deflections and with the canards removed to investigate the effects of the close-coupled canard on the high-angle-of-attack stability characteristics of the configuration. The results show that the canard adversely affected both static directional and lateral stability at high angles of attack to the point of making the basic configuration susceptible to yaw divergence in the region of maximum lift. A fuselage strake was developed which significantly improved static lateral-directional stability characteristics at high angles of attack while also increasing the maximum lift of the configuration. The strakes also enhanced pitch damping at high angles of attack; on the other hand, the strake degraded roll and yaw damping in the region of maximum lift.

INTRODUCTION

The potential performance benefits offered by the application of the close-coupled canard concept to maneuvering aircraft are well known and documented (refs. 1 to 5, for example). Over the past few years, there has been increasing interest in utilizing this technology in the next generation of combat aircraft. One particular application that has received attention involves integrating the canard with a wing and horizontal tail to form a three-surface arrangement. The potential performance advantages offered by such a configuration include reduced trimmed drag, lower structural weight, direct lift, and higher maximum lift coefficient. (See refs. 4 and 5.) Because very little data existed concerning the high-angle-of-attack (above 20°) characteristics of close-coupled canard designs, a broad research program was initiated several years ago at the NASA Langley Research Center to provide information on the high-angle-of-attack stability and control characteristics of this class of configurations. One configuration under study was designed by the McDonnell Aircraft Company and was derived from the basic F-15 design by attaching canard surfaces to a fairing assembly extending from the engine inlets. Static and dynamic wind-tunnel tests have been conducted on this configuration, and this report presents the results obtained.

SYMBOLS

The static longitudinal forces and moments are referred to the wind-axis system. All forced-oscillation and static lateral-directional data are referred to the body-axis system shown in figure 1. All data are referenced to a center-of-gravity position of 25.65 percent mean aerodynamic chord.

In order to facilitate international usage of data presented, dimensional quantities are presented both in the International System of Units (SI) and in U.S. Customary Units. Measurements and calculations were made in U.S. Customary Units. Conversion factors for the two systems may be found in reference 6.

b	wing span, m (ft)
$\bar{c}$	mean aerodynamic chord, m (ft)
C_A	axial-force coefficient, $F_A/q_\infty S$
C_D	drag coefficient, $F_D/q_\infty S$
C_L	lift coefficient, $F_L/q_\infty S$
C_l	rolling-moment coefficient, $M_X/q_\infty Sb$
C_m	pitching-moment coefficient, $M_Y/q_\infty S\bar{c}$
C_N	normal-force coefficient, $F_N/q_\infty S$
C_n	yawing-moment coefficient, $M_Z/q_\infty Sb$
C_Y	side-force coefficient, $F_Y/q_\infty S$
f	frequency of oscillation, Hz
F_A	axial force, N (lb)
F_D	drag force, N (lb)
F_L	lift force, N (lb)
F_N	normal force, N (lb)
F_Y	side force, N (lb)
I_X	moment of inertia about X body axis, kg-m^2 (slug-ft^2)
I_Z	moment of inertia about Z body axis, kg-m^2 (slug-ft^2)
k	reduced-frequency parameter, $\frac{\omega b}{2V}$ or $\frac{\omega \bar{c}}{2V}$
M_X	rolling moment, m-N (ft-lb)
M_Y	pitching moment, m-N (ft-lb)
M_Z	yawing moment, m-N (ft-lb)
p	roll rate, rad/sec
q	pitch rate, rad/sec
q_∞	dynamic pressure, Pa (lb/ft^2)
r	yaw rate, rad/sec
S	wing area, m^2 (ft^2)

u,v,w	components of resultant velocity V along X, Y, and Z body axes, respectively, m/sec (ft/sec)
V	free-stream velocity, m/sec (ft/sec)
X,Y,Z	body reference axes (fig. 1)
α	angle of attack, deg
$\dot{\alpha}$	rate of change of angle of attack, rad/sec
β	angle of sideslip, deg
$\dot{\beta}$	rate of change of angle of sideslip, rad/sec
δ_c	canard deflection angle, positive for trailing edge down, deg
δ_h	horizontal-tail deflection angle, deg
θ	angle of pitch, deg
ϕ	angle of roll, deg
ψ	angle of yaw, deg
ω	angular frequency, $2\pi f$, rad/sec

Derivatives:

$$C_{m_\alpha} = \frac{\partial C_m}{\partial \alpha}$$

$$C_{l_\beta} = \frac{\partial C_l}{\partial \beta} \qquad C_{n_\beta} = \frac{\partial C_n}{\partial \beta} \qquad C_{Y_\beta} = \frac{\partial C_Y}{\partial \beta}$$

$$C_{n_{\beta,dyn}} = C_{n_\beta} \cos \alpha - \frac{I_Z}{I_X} C_{l_\beta} \sin \alpha$$

$$C_{l_p} = \frac{\partial C_l}{\partial \frac{pb}{2V}} \qquad C_{n_p} = \frac{\partial C_n}{\partial \frac{pb}{2V}} \qquad C_{Y_p} = \frac{\partial C_Y}{\partial \frac{pb}{2V}}$$

$$C_{l_{\dot{\beta}}} = \frac{\partial C_l}{\partial \frac{\dot{\beta} b}{2V}} \qquad C_{n_{\dot{\beta}}} = \frac{\partial C_n}{\partial \frac{\dot{\beta} b}{2V}} \qquad C_{Y_{\dot{\beta}}} = \frac{\partial C_Y}{\partial \frac{\dot{\beta} b}{2V}}$$

$$C_{l_r} = \frac{\partial C_l}{\partial \frac{rb}{2V}} \qquad C_{n_r} = \frac{\partial C_n}{\partial \frac{rb}{2V}} \qquad C_{Y_r} = \frac{\partial C_Y}{\partial \frac{rb}{2V}}$$

$$C_{m_q} = \frac{\partial C_m}{\partial \frac{q\bar{c}}{2V}} \qquad C_{N_q} = \frac{\partial C_N}{\partial \frac{q\bar{c}}{2V}} \qquad C_{A_q} = \frac{\partial C_A}{\partial \frac{q\bar{c}}{2V}}$$

$$C_{m_{\dot{\alpha}}} = \frac{\partial C_m}{\partial \frac{\dot{\alpha}\bar{c}}{2V}} \qquad C_{N_{\dot{\alpha}}} = \frac{\partial C_N}{\partial \frac{\dot{\alpha}\bar{c}}{2V}} \qquad C_{A_{\dot{\alpha}}} = \frac{\partial C_A}{\partial \frac{\dot{\alpha}\bar{c}}{2V}}$$

MODEL AND TESTS

A three-view sketch of the model used in the tests is shown in figure 2, and a photograph of the model mounted in the wind tunnel is shown in figure 3. The model was obtained by modifying an existing 0.10-scale model of the F-15 airplane. The primary modifications were the incorporation of close-coupled canards and fuselage fairing, or "shelves," on which the canards were mounted. The canard leading-edge sweep was 50°, and the ratio of canard to wing area was 0.10. The inlet cowls were fixed at 11° leading edge down. Other geometric characteristics of the model are presented in table I.

The static-force tests were conducted at the Langley Research Center in a low-speed wind tunnel with a 12-foot octagonal test section. The tests were made with the setup shown in figure 4. The model was sting mounted on a six-component, internally mounted strain-gage balance. The engine inlets and exits were open to allow flow through the model for the tests which were conducted at a tunnel speed of 17.7 m/sec (58 ft/sec), corresponding to a Reynolds number of 0.59×10^6 based on the wing mean aerodynamic chord. Data were obtained through angle-of-attack and angle-of-sideslip ranges of 0° to 85° and -10° to 10°, respectively.

Dynamic forced-oscillation tests were conducted in the Langley 30- by 60-Foot Tunnel with the setups shown in figure 5. The model was sting mounted on the same six-component internal strain-gage balance used for the static-force tests. Detailed descriptions of the forced-oscillation equipment and associated data-reduction system are contained in reference 7. The tests were conducted at a tunnel speed of 28 m/sec (91.7 ft/sec), corresponding to a Reynolds number of 0.92×10^6 based on the wing mean aerodynamic chord. Data were obtained through an angle-of-attack range of 0° to 60°. The pitch-oscillation tests were conducted at an amplitude of ±5° for reduced frequencies of 0.043 and 0.021, while the roll and yaw tests were conducted at the same amplitude for reduced frequencies of 0.15, 0.11, and 0.07. Some roll and yaw data were also obtained at an amplitude of ±10°.

The static-force tests were conducted with the canard incidence varying from -60° to 18°. The forced-oscillation tests were conducted with the canard incidence varying from 0° to -25°. Limited component buildup data were also obtained.

RESULTS AND DISCUSSION

Static Characteristics

Baseline configuration.- The neutral-controls longitudinal aerodynamic characteristics of the model with and without the canards are presented in figure 6. The data show that adding the canards to the configuration increased the lift-curve slope and the maximum lift attained. However, maximum lift occurred at a lower angle of attack with the canards on than with them off (27° versus 34°).

The canard-off pitching-moment data exhibit essentially neutral stability at low angles of attack followed by an increase in stability at the higher angles of attack. As expected, addition of the canards causes the configuration to be statically unstable at the low to moderate angles of attack (Static margin = -0.08). Above $\alpha = 27°$, however, the pitching-moment data exhibit a sharp stable break caused by a combination of canard stall and flow separation on the fuselage shelf inboard of the canards. The effect of sideslip on pitching moment is shown in figure 7. The data indicate no significant effect.

The effect of canard incidence on the longitudinal characteristics is shown in figure 8. In the low to moderate angle-of-attack range, the data show the expected effects of canard deflection on lift and pitching moment. Unloading the canard delays occurrence of maximum lift to higher angles of attack and reduces the magnitude of the stable pitching-moment break above stall. Deflecting the canard up to -24° increases the value of maximum lift in the higher angle-of-attack range.

The static lateral-directional stability characteristics of the model with neutral controls with and without the canards are presented in figure 9 in terms of the derivatives C_{Y_β}, C_{l_β}, and C_{n_β}. The data were obtained by sloping the force and moment data over a sideslip range of ±5°. The canard-off data show that directional stability reduces steadily above 5° angle of attack such that unstable characteristics are exhibited above $\alpha = 22°$. As expected, addition of the canard reduces stability in the low to moderate angle-of-attack range. However, the data show that this degradation in stability persists to beyond $\alpha = 40°$, resulting in highly unstable values of C_{n_β} for angles of attack above about 25°. This characteristic is detrimental to high-angle-of-attack flying qualities and departure/spin resistance.

The lateral stability data show that the canard-off configuration exhibits a high level of lateral stability throughout the angle-of-attack range. Addition of the canard results in minor effects on C_{l_β} except in the 25° to 40° angle-of-attack range, where the canard configuration exhibits a sharp loss in lateral stability. This characteristic is examined further in figure 10, which shows the variation of C_Y, C_n, and C_l with sideslip at angles of attack of 25°, 30°, and 35°. At $\alpha = 25°$, the data show linear and stable variations of C_l with β for both canard-on and canard-off configurations. However, at $\alpha = 30°$, the canard-on configuration exhibits highly nonlinear characteristics with a very abrupt unstable variation in rolling moment over a small sideslip range near $\beta = 0°$. On the other hand,

with the canard removed, the characteristics are stable and fairly linear. At $\alpha = 35°$, both configurations exhibit stable characteristics, although the canard-on data still show a significant degree of nonlinearity and lower stability. At first, it was thought that this instability was caused by an unfavorable interaction between the forebody-generated vortices and the canard-wing flow field. To test this hypothesis, the pointed, slender nose of the configuration was replaced by a short blunt nose, as illustrated in figure 11. As indicated by the data shown, this drastic modification did not significantly alter the loss in lateral stability. These results suggest that the forebody flow is not a significant factor in causing the instability.

Flow-visualization tests using surface tufts were subsequently conducted in an attempt to further understand the flow mechanisms involved. Figure 12 shows two photographs taken during this study at $\alpha = 30°$ and $\beta = 0°$ and $-5°$. The photographs reveal that the loss in static lateral stability is caused by the interaction of the canard with the outboard region of the fuselage, which for convenience, will be referred to as the shelf. At $\beta = 0°$, the tuft patterns indicate essentially symmetric flow conditions over the entire upper surface of the configuration. At $\beta = -5°$, however, massive separation occurs on the windward shelf, particularly in the region just aft of the canard. On the other hand, the flow over the leeward shelf appears to be significantly less separated. The resulting asymmetric lift distribution causes a rolling-moment increment into the sideslip which is destabilizing. This loss in lateral stability combined with the highly unstable directional-stability characteristics makes the configuration highly susceptible to yaw divergence, as shown by the data presented in figure 13. Plotted are the variations of the parameter $C_{n_{\beta,dyn}}$ with and without the canards. Negative values of $C_{n_{\beta,dyn}}$ indicate susceptibility to directional divergence. The configuration without the canards exhibits positive values of this parameter throughout the angle-of-attack range, indicating good resistance to departure. Addition of the canards results in a sharp drop in $C_{n_{\beta,dyn}}$ such that negative values occur in the 27° to 35° angle-of-attack range. These results indicate that the configuration has high susceptibility to yaw divergence. In an attempt to correct this problem, a number of configuration modifications were studied. The results are discussed in the next section.

The effect of canard incidence on the static lateral-directional stability characteristics is summarized in figure 14. The results show no large effect on directional stability. However, deflecting the canard trailing edge up significantly improves lateral stability in the region around $\alpha = 30°$. Tuft-flow visualization indicates that unloading the canard significantly improves the flow over the shelf region inboard and aft of the canard, particularly under sideslip. The data of figure 14 show that a canard deflection of $-36°$ eliminates the instability problem. Thus, a potential method for enhancing lateral stability in the region of maximum lift is to schedule the canard deflection such that by $\alpha = 30°$, it is deflected to at least $-30°$. A drawback of this approach could be the loss in trimmed lift resulting from excessively large trailing-edge-up canard deflections; however, in this instance only a minor loss in trimmed lift was measured.

Modified configuration.- In an attempt to find alternative solutions to the lateral-stability problem, various wing fences, wing leading-edge devices, nose strakes, and fuselage strakes were tested. Some of these modifications improved lateral stability but were very detrimental to lift. The only modification that enhanced both stability and lift characteristics was a comparatively large pair of fuselage strakes mounted adjacent to the canopy at a radial location of 37.5° above

the maximum half-breadth of the forebody. (See fig. 15.) Additional work would be required to minimize the size and to optimize the shape of the strakes before placing them on a full-scale airplane.

The effects of these strakes on static-longitudinal characteristics are shown in figure 16. The lift data show that the strakes have essentially no effect up to $\alpha = 27°$, which is where maximum lift occurs on the basic configuration. In the 27° to 35° angle-of-attack region, addition of the strakes results in a small increase in lift, suggesting that the strakes are delaying flow separation on the fuselage shelf. This effect is also indicated by the pitching-moment data, which show that the strong stable break (high values of negative C_{m_α}) above $\alpha = 27°$ exhibited by the basic airplane is significantly reduced with the strakes added.

The effects of the fuselage strakes on static lateral-directional stability are shown in figure 17. In the 15° to 25° angle-of-attack range, the strakes degrade directional stability, whereas in the 30° to 40° range, they provide a significant improvement in stability. Examination of the C_{Y_β} data suggests that this enhancement of C_{n_β} is a result of favorable flow interaction with the vertical tails such that their effectiveness is maintained to higher angles of attack. The lateral stability results show that in the 27° to 37° angle-of-attack range, the strakes provide a dramatic improvement in C_{l_β} such that the instability is eliminated. The tuft photographs in figure 18 verify that the cause of this increase in stability is the reattachment of the flow over the windward fuselage shelf under sideslip conditions. Figure 19 shows the effect of the strakes on the variation of C_Y, C_n, and C_l with sideslip at angles of attack of 25°, 30°, and 35°. At $\alpha = 25°$, the data show that the strakes cause a reduction in directional stability without significantly affecting lateral stability. On the other hand, at $\alpha = 30°$, the strakes have no effect on directional stability while providing a dramatic improvement in lateral stability. The strakes provide a fairly linear, highly stable variation of rolling moment with sideslip. At $\alpha = 35°$, the data show that the strakes improve both directional and lateral stability. Furthermore, these results are in agreement with those obtained in the Langley 16-Foot Transonic Tunnel for Mach numbers up to 0.90 (cf. ref. 8).

The beneficial effect of the fuselage strakes on departure resistance is summarized in figure 20, which shows the variation of $C_{n_{\beta,dyn}}$ with angle of attack with and without the strakes. As expected, the improvements in C_{n_β} and C_{l_β} around $\alpha = 30°$ provided by the strakes result in a large increase in the values of $C_{n_{\beta,dyn}}$ such that the parameter remains positive throughout the angle-of-attack range, indicating that the configuration should be resistant to yaw divergence.

Damping Characteristics

Pitch.- The results of the pitch forced-oscillation tests of the basic configuration with neutral controls are summarized in figure 21. The results show that the configuration exhibits stable pitch damping up to $\alpha = 20°$ followed by a sharp loss in damping such that unstable characteristics are encountered above $\alpha = 25°$. The

effects of deflecting the canard or removing it are shown in figure 22. Comparison of the canard-on and canard-off data indicates that at lower angles of attack, the canard enhances damping, as expected, since the canard adds planform area to the configuration. However, at the higher angles of attack, above about 25°, the canard is detrimental to damping. This characteristic is believed to be due to two effects. First, the canard itself produces a destabilizing increment because above stall, the canard is operating in a region of negative lift-curve slope. Second, as discussed earlier, the presence of the canard adversely affects the flow over the fuselage shelf, causing premature separation and lift loss. As expected, both of these adverse effects can be alleviated by unloading the canard. As shown in figure 22, deflecting the canard to -25° significantly reduces the loss in pitch damping in the 25° to 35° angle-of-attack region.

As discussed earlier, addition of the fuselage strakes enhanced lateral stability by improving the flow over the fuselage shelf. Based on the above discussion, it would be expected, therefore, that the strakes would also be beneficial to pitch damping in the 25° to 35° angle-of-attack range. Figure 23 bears this out by comparing data measured with and without the strakes. The effect of combining the beneficial effects of the strakes and unloading the canard to -25° is shown in figure 24. The data show that this configuration exhibits damped characteristics throughout the angle-of-attack range shown except at $\alpha = 45°$, where the damping is essentially neutral.

The contribution of the horizontal tail to pitch damping is shown in figure 25. The data indicate that up to 30°, the tail has only a small effect on damping, while at the higher angles of attack above 30°, the tail contributes significantly to damping. Unloading the tail to -25° further enhances this effect.

Roll.- The effects of oscillation frequency and amplitude on the roll-oscillation derivatives measured with neutral controls are presented in figures 26 and 27, respectively. The data show that the configuration has stable roll-damping characteristics beyond maximum lift up to $\alpha = 35°$, above which there is an abrupt decrease in damping to very low values. The results also indicate that there are no significant effects of oscillation frequency or amplitude.

The canard contributions to the roll-damping characteristics are shown in figure 28. The data indicate that the canard effects on the damping are relatively small throughout the angle-of-attack range. The effects of deflecting the canard are shown in figure 29. As would be expected based on the canard-off results, varying canard incidence does not significantly change the roll-damping characteristics of the configuration. These results suggest that the wing dominates these characteristics and indicate that the coupling between the canard and wing flow fields at high angles of attack is not strong.

The effect of adding the fuselage strakes is shown in figure 30. Consistent with the static stability results discussed earlier, the data indicate no significant effect up to $\alpha = 25°$. Above $\alpha = 25°$, the strakes add a significant negative increment to the cross derivative $C_{n_p} + C_{n_\beta} \sin \alpha$. This is an undesirable characteristic in that it will degrade Dutch roll stability. The roll-damping data show that the strakes degrade roll damping in the 27° to 37° range and enhance damping in the 37° to 47° range. This effect is exactly opposite to the effect on static lateral stability; as discussed earlier, the strakes dramatically enhance C_{l_β} in the $\alpha = 27°$ to 37° range while slightly reducing stability in the $\alpha = 37°$ to 47°

range. The combination of high static lateral stability, low-roll damping, and adverse yaw due to roll rate would be expected to make the configuration with the fuselage strakes susceptible to undamped lateral-directional oscillations or, "wing rock," in the 30° angle-of-attack range. Figure 31 shows that, as expected, varying canard incidence does not significantly alter the roll-damping characteristics of this configuration.

As shown in figure 32, the vertical tails do not significantly affect roll damping throughout the angle-of-attack range of the tests.

Yaw.- Yaw forced-oscillation results for the basic configuration with neutral controls are shown in figure 33. The data indicate that the configuration exhibits stable yaw-damping characteristics throughout the test angle-of-attack range. The contribution of the vertical tails to these characteristics is shown in figure 34. The tails provide most of the damping up to $\alpha = 25°$. The minimum damping exhibited by the basic configuration at $\alpha = 30°$ is due to the loss in vertical-tail effectiveness in the 30° to 37° range. In the $\alpha = 38°$ to 45° range, the tails again provide a significant stabilizing increment to yaw damping. Further insight into the mechanism causing this effect can be gained by examining the data shown in figure 35 for the configuration with and without the canards. The large increase in yaw damping in the $\alpha = 38°$ to 45° range disappears if the canards are removed. This result suggests a favorable flow interaction between the canards and the vertical tails which reestablishes the effectiveness of the latter surfaces in providing damping in this high-angle-of-attack region. Data at other angle-of-attack conditions indicate no significant effect of the canards on yaw damping. Figure 36 shows the effect of deflecting the canards to -25°. The data indicate that the primary effect is to delay the initial loss in vertical-tail effectiveness and hence damping by 5° in angle of attack, from 30° to 35°. The subsequent recovery of vertical-tail effectiveness is also delayed by the same increment in angle of attack.

The effect of the fuselage strakes on yaw-damping characteristics is shown in figure 37. The data show that addition of the strakes enhances damping in the 15° to 30° angle-of-attack range. However, above 30°, the effect is detrimental and results in unstable yaw-damping characteristics with the canard at zero incidence. Comparison with the strake-off data suggests that addition of the strakes eliminates the favorable contribution of the vertical tail in the $\alpha = 40°$ region, as discussed earlier. The unfavorable influence of the fuselage strakes can be minimized by deflecting the canard to -25°.

The results of this and other studies (see ref. 9) on three-surface configurations illustrate the strong configuration dependence of these designs. As a result, it is felt that the results presented in this report are applicable to the test configuration only; generalization of these results to other three-surface concepts should be approached with caution.

CONCLUSIONS

The results of a wind-tunnel study of the static and dynamic characteristics of a three-surface fighter concept based on the F-15 airplane can be summarized as follows:

1. Compared with the canard-off configuration, addition of the close-coupled canard increases the maximum lift attained while reducing the angle of attack at which maximum lift occurs.

2. The lift produced by the canard in front of the center of gravity causes the configuration to be statically unstable in pitch at the low to moderate angles of attack; however, a desirable strong stable break occurs at maximum lift as a result of canard and fuselage shelf stall.

3. The canard adversely affects both static directional and lateral stability at high angles of attack. Of particular concern are the sharp reduction in the effective dihedral parameter to unstable values in the 30° angle-of-attack region and the resultant high susceptibility of the configuration to yaw divergence. This loss in stability is a result of the canard causing massive flow separation over the windward fuselage shelf under sideslip. Deflecting the canard trailing edge up alleviates this adverse effect.

4. Addition of fuselage strakes mounted just below the canopy significantly improves static lateral-directional stability in the 25° to 40° angle-of-attack range. A small increase in lift also results.

5. The canard enhances pitch damping at the low to moderate angles of attack. However, once the canard stalls, the effect on pitch damping is highly adverse.

6. The fuselage strakes increase pitch damping in the 25° to 35° angle-of-attack range by favorably interacting with the flow over the fuselage shelf at these conditions.

7. The basic configuration exhibits good roll-damping characteristics up to angles of attack beyond maximum lift. The canard does not have a strong effect on these characteristics. The fuselage strakes also do not significantly affect roll damping except in the 30° to 35° angle-of-attack range, where they reduce the damping significantly. The strakes also cause a large negative increment in the roll-damping cross derivative $C_{n_p} + C_{n_\beta} \sin \alpha$ in this angle-of-attack range. The combination of low roll damping and adverse yaw due to roll would be expected to make the configuration prone to wing rock in the maximum-lift region.

8. The basic configuration exhibits good yaw-damping characteristics throughout the test angle-of-attack range. The canard does not strongly affect these characteristics except in the 38° to 45° angle-of-attack range, where it significantly enhances yaw damping by increasing vertical-tail effectiveness. The fuselage strakes increase damping up to angles of attack of 30° and degrade damping at the higher angles of attack.

Langley Research Center
National Aeronautics and Space Administration
Hampton, VA 23665
January 12, 1983

REFERENCES

1. Behrbohm, Hermann: Basic Low Speed Aerodynamics of the Short-Coupled Canard Configuration of Small Aspect Ratio. SAAB TN 60, Saab Aircraft Co. (Linköping, Sweden), July 1965.

2. Lacey, David W.: Aerodynamic Characteristics of the Close-Coupled Canard as Applied to Low-to-Moderate Swept Wings. U.S. Navy, Jan. 1979.
   Volume 1: General Trends. DTNSRDC-79/001. (Available from DTIC as AD A063 819.)
   Volume 2: Subsonic Speed Regime. DTNSRDC-79/002. (Available from DTIC as AD A067 122.)

3. Gloss, Blair B.; and McKinney, Linwood W.: Canard-Wing Lift Interference Related to Maneuvering Aircraft at Subsonic Speeds. NASA TM X-2897, 1973.

4. Agnew, J. W.; and Hess, J. R., Jr.: Benefits of Aerodynamic Interaction to the Three Surface Configuration. AIAA Paper 79-1830, Aug. 1979.

5. Agnew, J. W.; Lyerla, G. W.; and Grafton, S. B.: The Linear and Nonlinear Aerodynamics of Three-Surface Aircraft Concepts. J. Aircr., vol. 18, no. 11, Nov. 1981, pp. 956-962.

6. Standard for Metric Practice. E 380-79, American Soc. Testing & Mater., c.1980.

7. Chambers, Joseph R.; and Grafton, Sue B.: Static and Dynamic Longitudinal Stability Derivatives of a Powered 1/9-Scale Model of a Tilt-Wing V/STOL Transport. NASA TN D-3591, 1966.

8. Henderson, William P.; and Leavitt, Laurence D.: Stability and Control Characteristics of a Three-Surface Advanced Fighter Configuration at Angles of Attack up to 45°. NASA TM-83171, 1981.

9. Croom, Mark A.; Grafton, Sue B.; and Nguyen, Luat T.: High Angle-of-Attack Characteristics of Three-Surface Fighter Aircraft. AIAA-82-0245, Jan. 1982.

TABLE I.- GEOMETRIC CHARACTERISTICS OF MODEL

Overall fuselage length, m (ft)	1.91 (6.25)
Moments of inertia:	
I_X, kg-m^2 (slug-ft^2)	0.369 (0.272)
I_Z, kg-m^2 (slug-ft^2)	2.602 (1.919)
Wing:	
Span, m (ft)	1.31 (4.28)
Area, m^2 (ft^2):	
Theoretical	0.566 (6.09)
Reference	0.565 (6.08)
Mean aerodynamic chord, m (ft)	0.486 (1.59)
Aspect ratio	3.01
Taper ratio	0.25
Sweepback of leading edge, deg	45
Dihedral, deg	-1
Incidence, deg	0
Ailerons:	
Span (percent b/2)	25.3
Area (each), m^2 (ft^2)	0.0124 (0.133)
Flaps:	
Type	Single slotted
Area (each), m^2 (ft^2)	0.017 (0.18)
Canards:	
Span, m (ft)	0.187 (0.613)
Area (each), m^2 (ft^2)	0.028 (0.300)
Mean aerodynamic chord, m (ft)	0.167 (0.549)
Aspect ratio	3.007
Taper ratio	0.25
Sweepback of leading edge, deg	50
Dihedral, deg	20
Hinge-line location, percent chord	25
Horizontal tails:	
Span, m (ft)	0.239 (0.783)
Area (each), m^2 (ft^2)	0.056 (0.60)
Aspect ratio	2.05
Taper ratio	0.34
Sweepback of leading edge, deg	40
Dihedral, deg	0
Hinge-line location, percent chord	60.9
Vertical tails:	
Span, m (ft)	0.315 (1.032)
Area (each), m^2 (ft^2)	0.0582 (0.626)
Taper ratio	0.266
Sweepback of leading edge, deg	36.57
Rudders (each):	
Area, m^2 (ft^2)	0.00948 (0.102)
Hinge-line location, percent chord	71.75

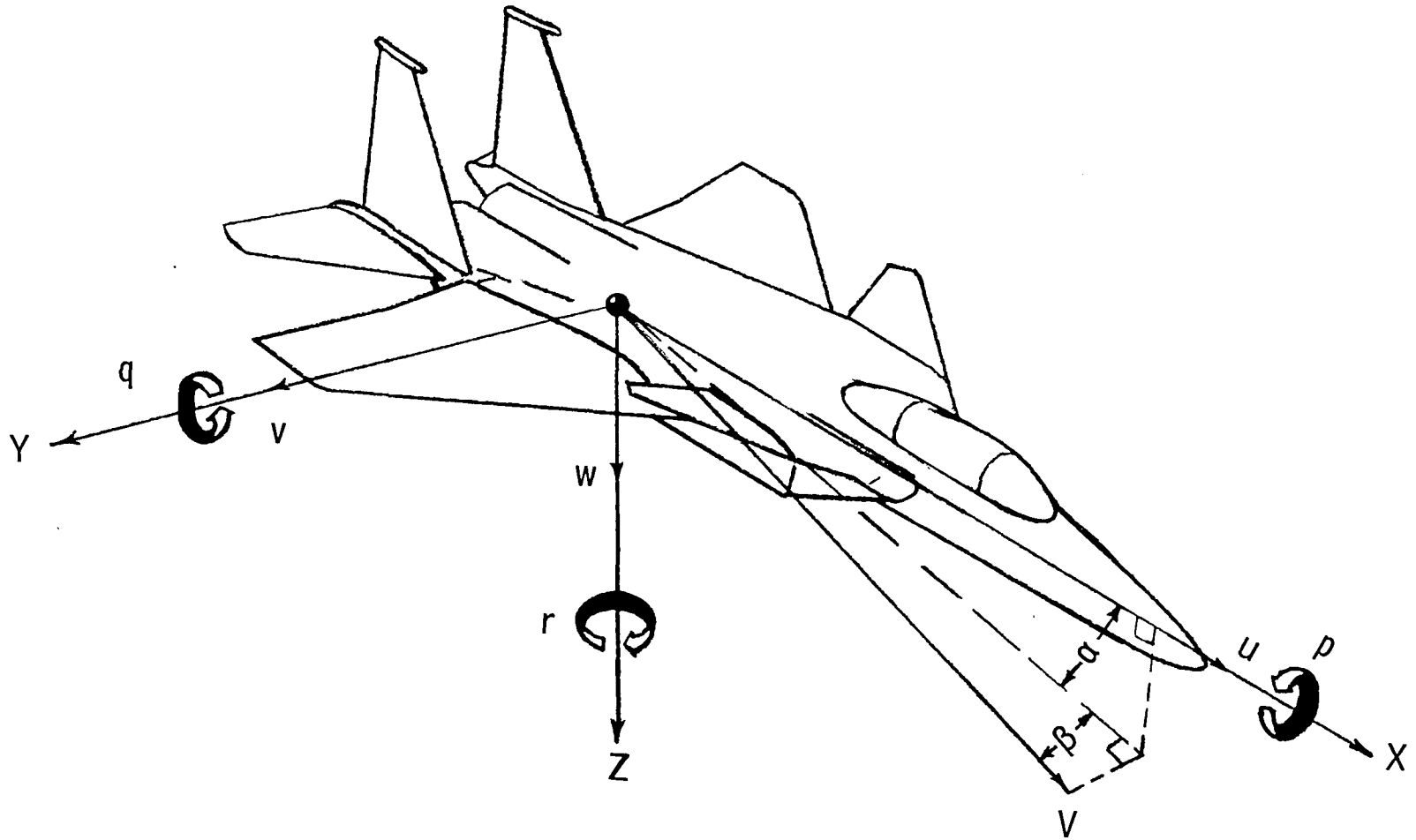

Figure 1.- The body system of axes.

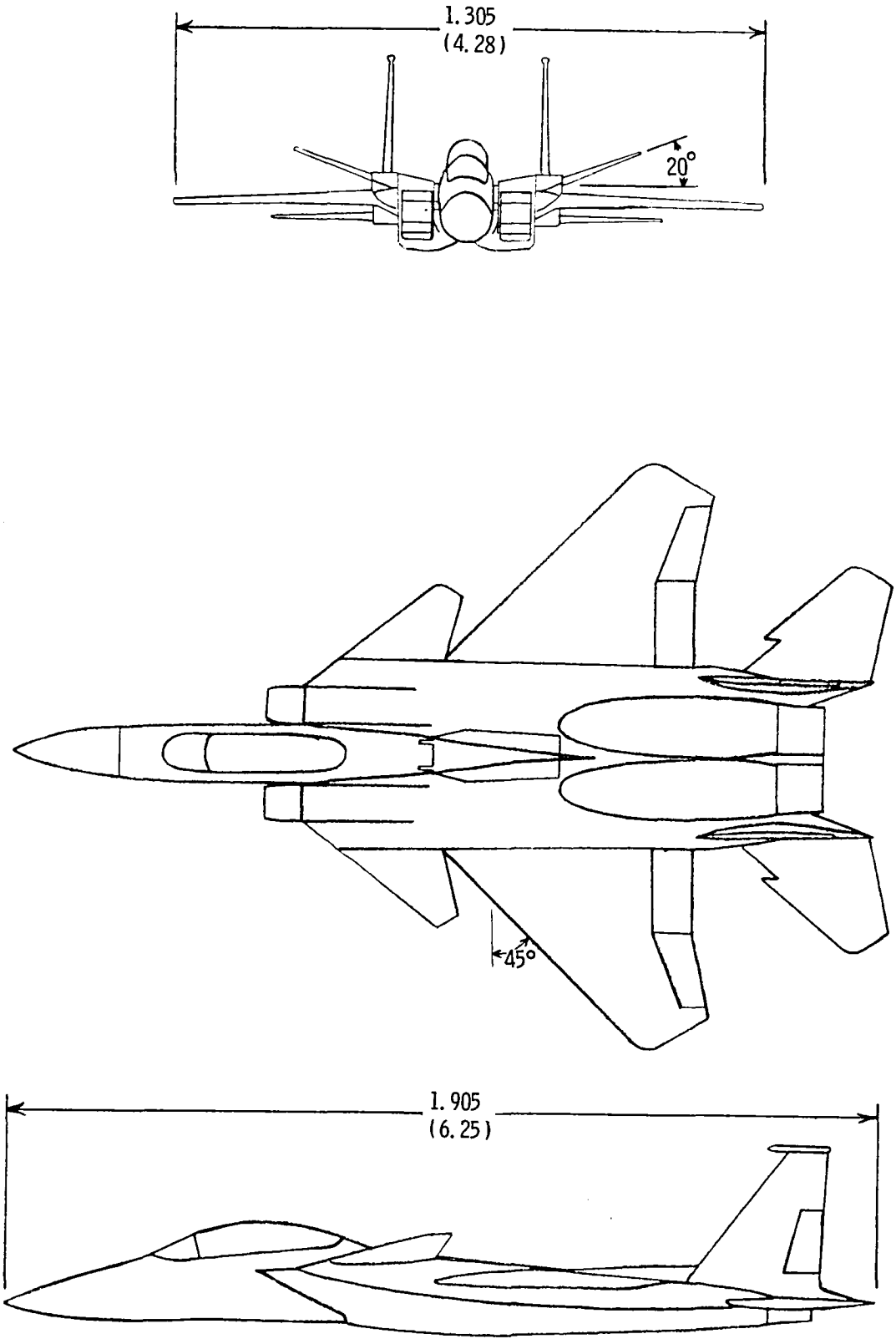

Figure 2.- Three-view sketch of model. Dimensions are given in meters (feet) unless otherwise indicated.

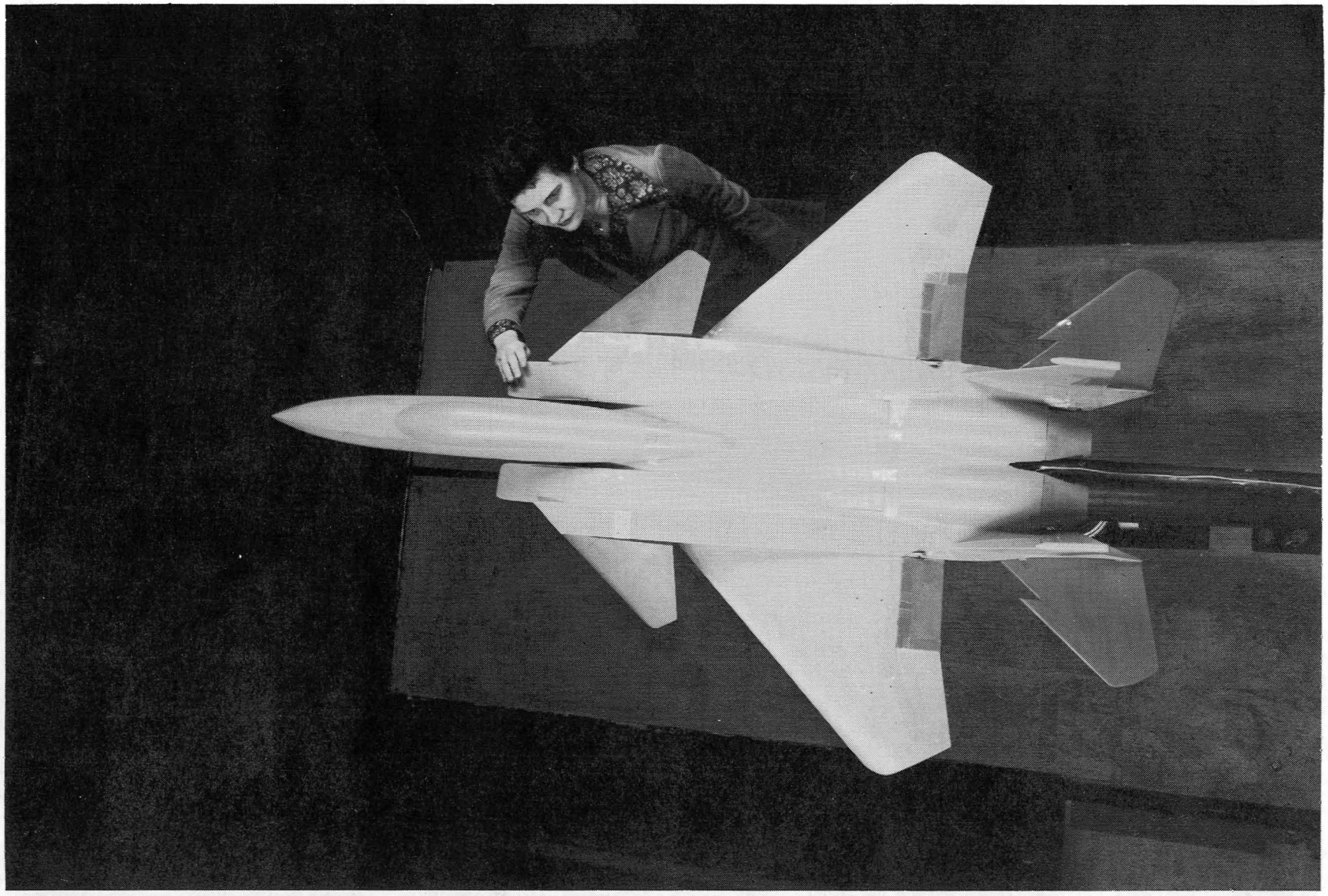

L-80-1815

Figure 3.- Photograph of model mounted for static-force tests.

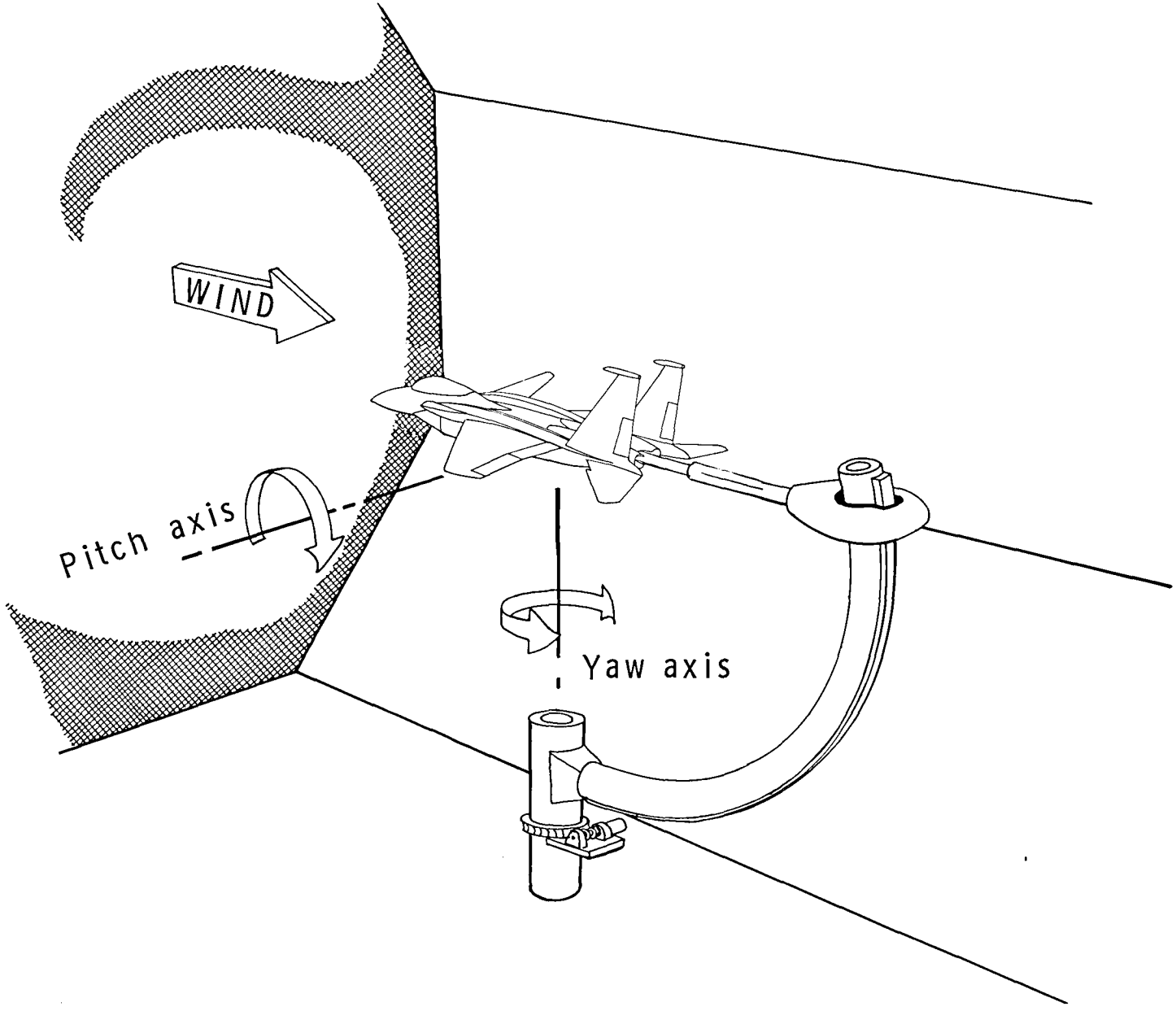

Figure 4.- Schematic diagram of model mounted for static-force tests.

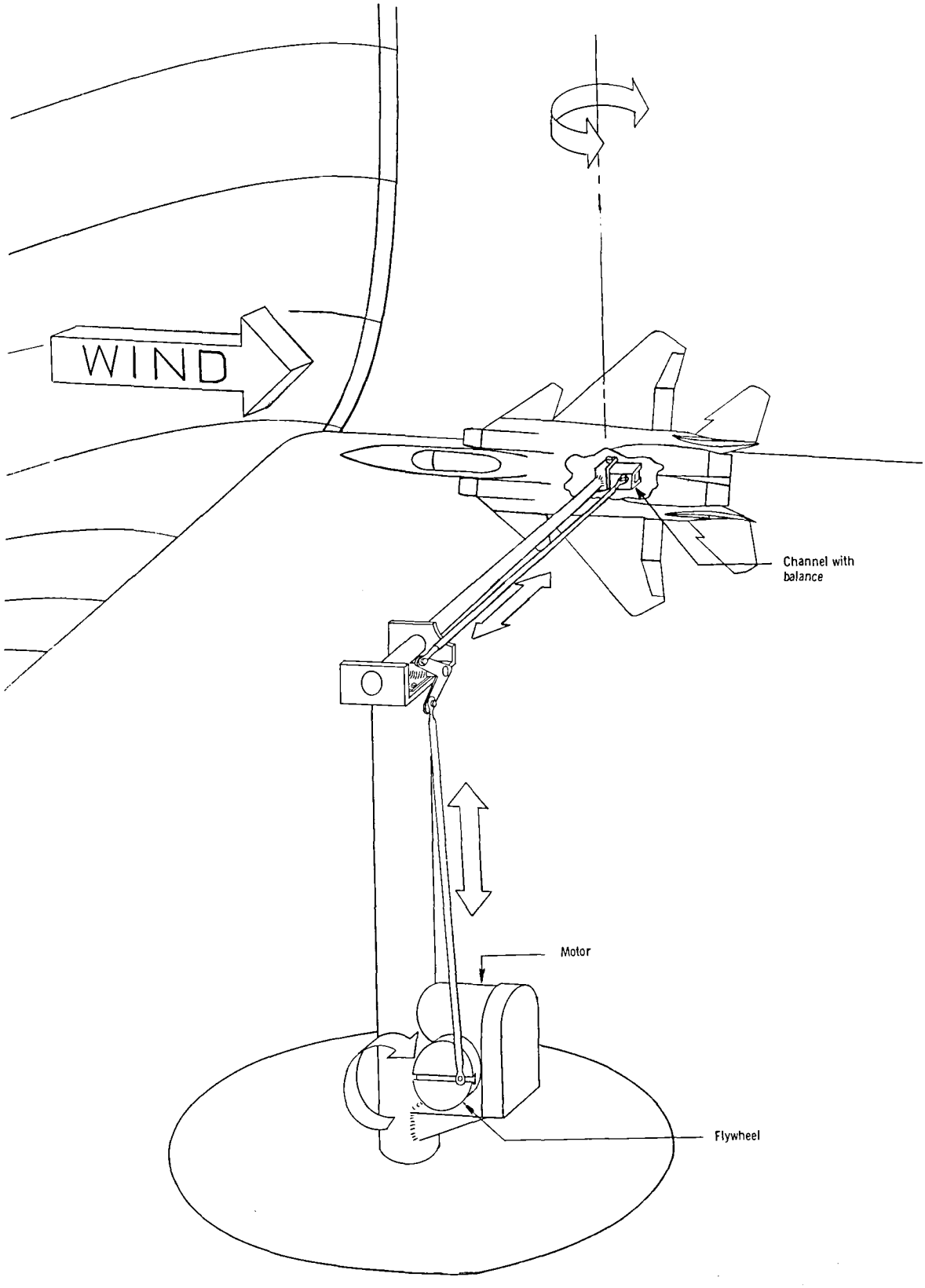

(a) Pitching setup.

Figure 5.- Schematic diagrams of model mounted for oscillatory-force tests.

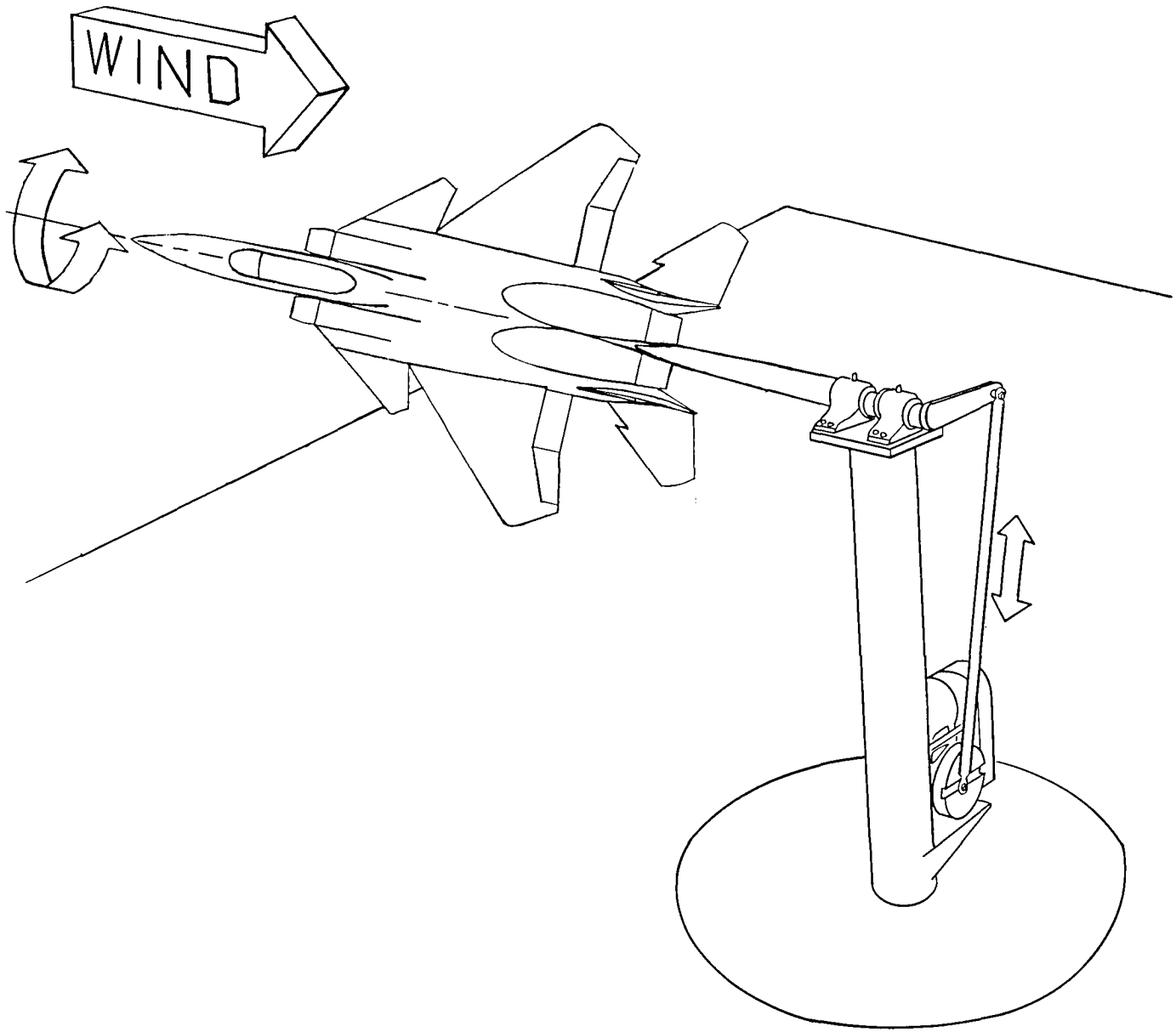

(b) Rolling setup.

Figure 5.- Continued.

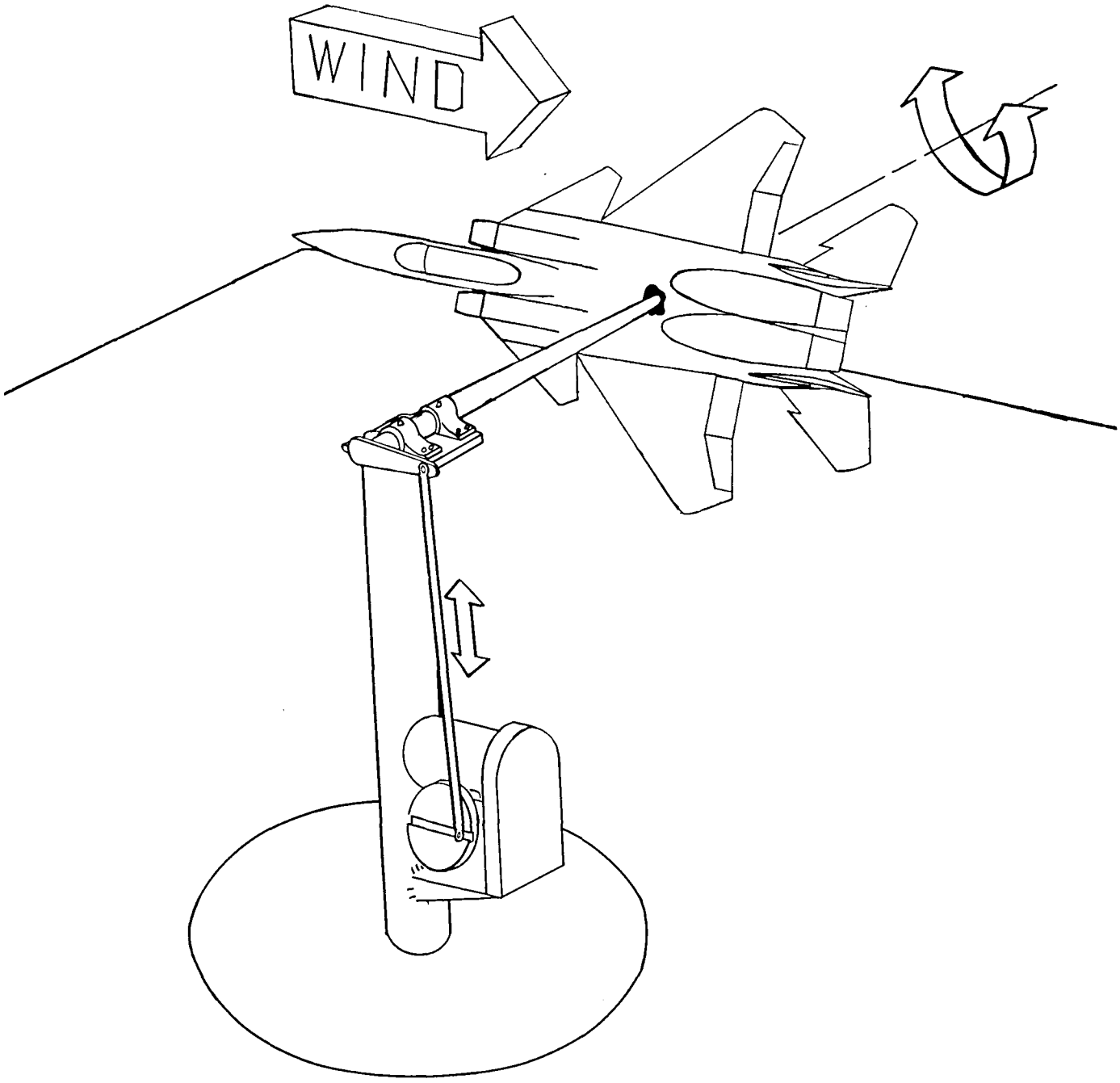

(c) Yawing setup.

Figure 5.- Concluded.

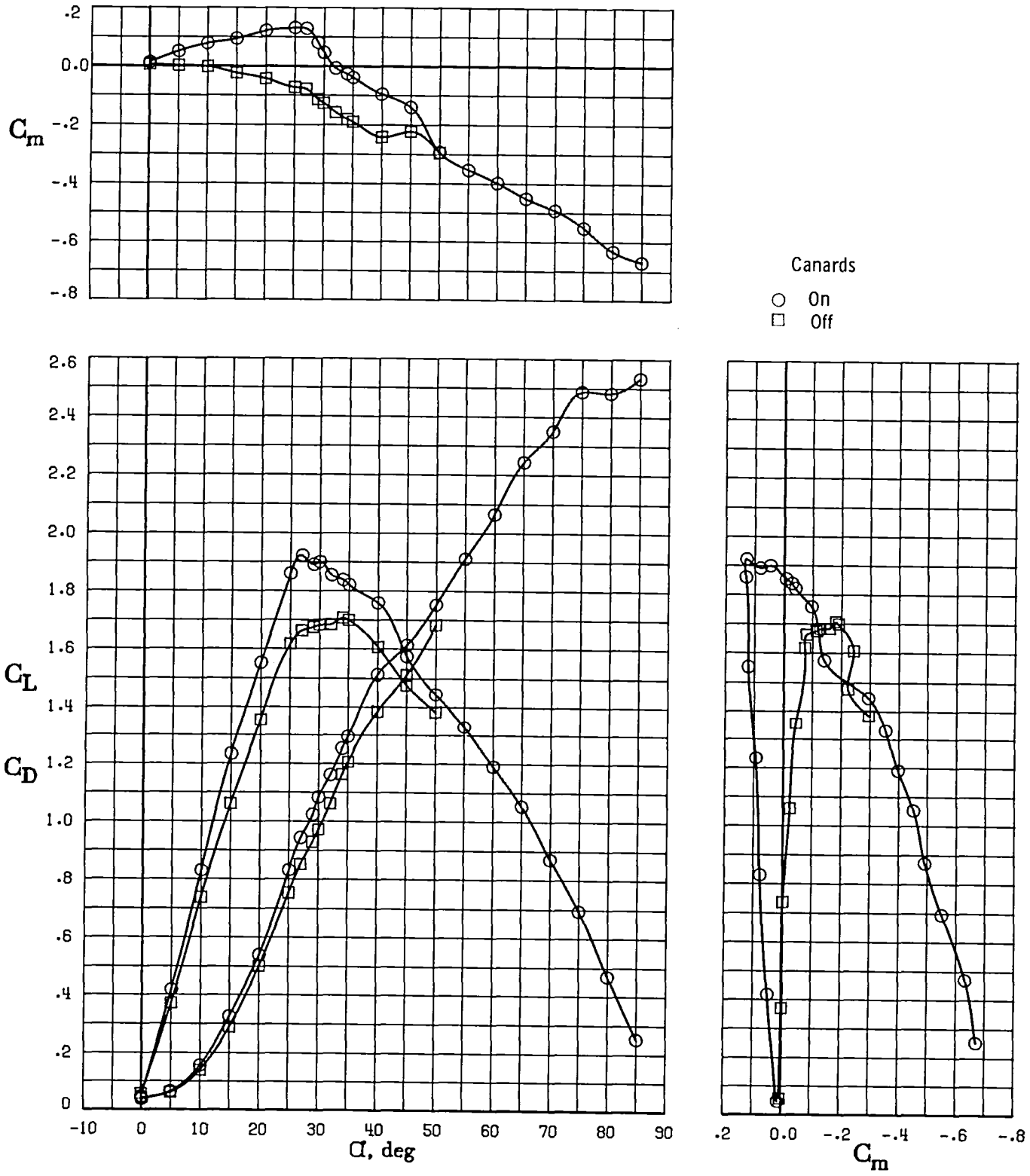

Figure 6.- Effect of canards on static longitudinal characteristics. $\delta_c = 0°$.

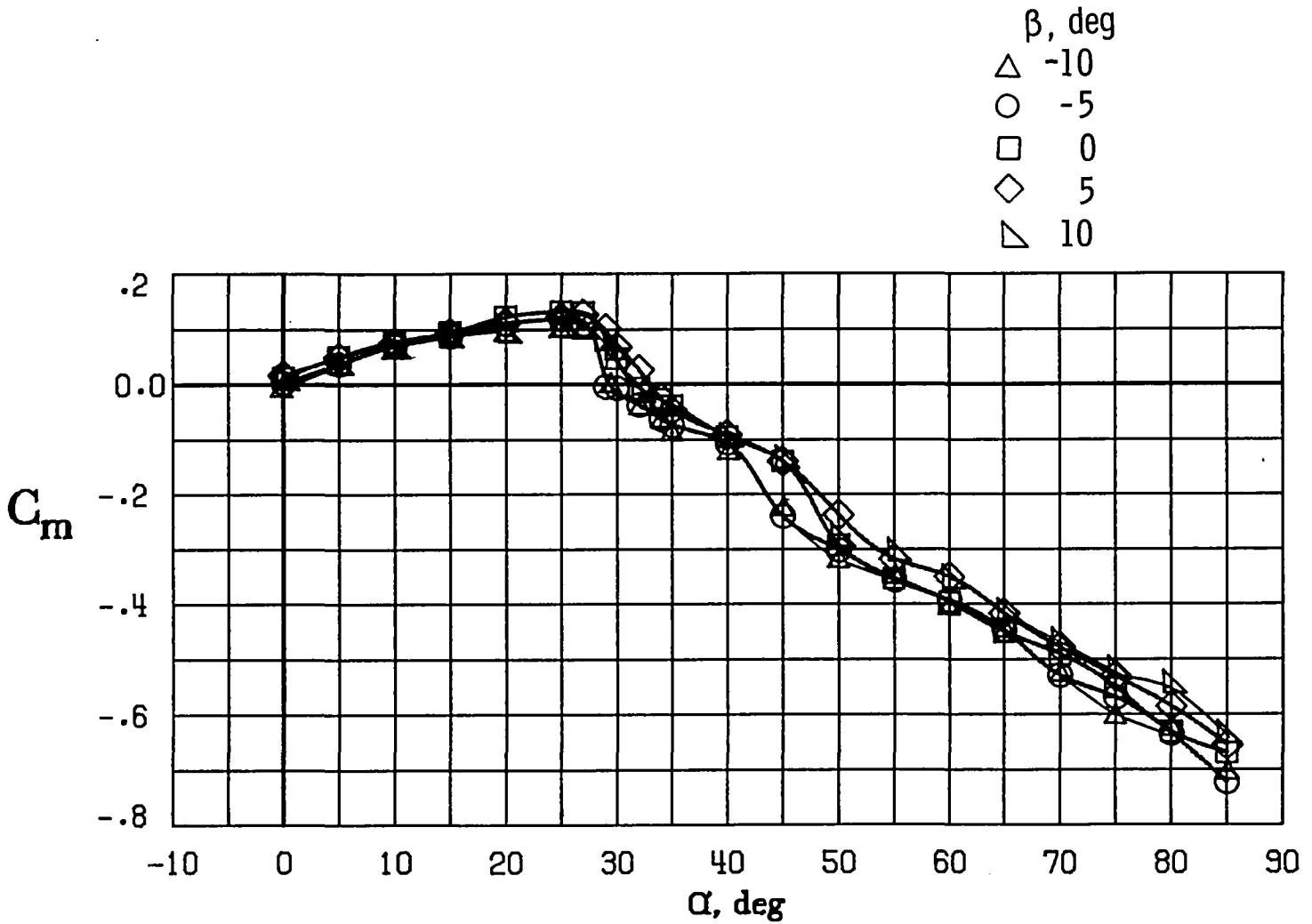

Figure 7.- Effect of sideslip on pitching moment. Center of gravity = 25.65 percent $\bar{c}$; $\delta_c = 0°$.

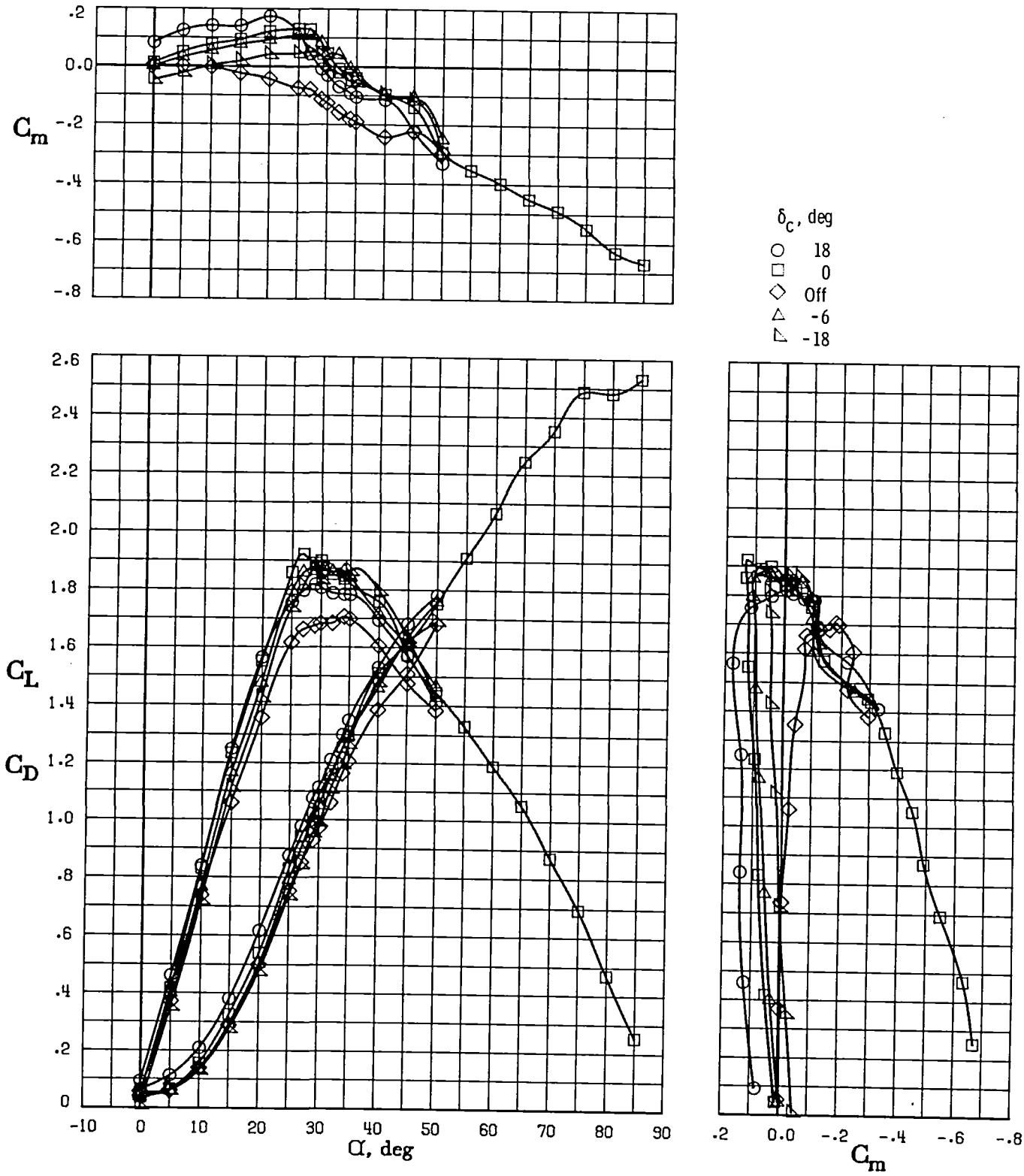

(a) Moderate deflections.

Figure 8.- Effect of canard deflection on static longitudinal characteristics.

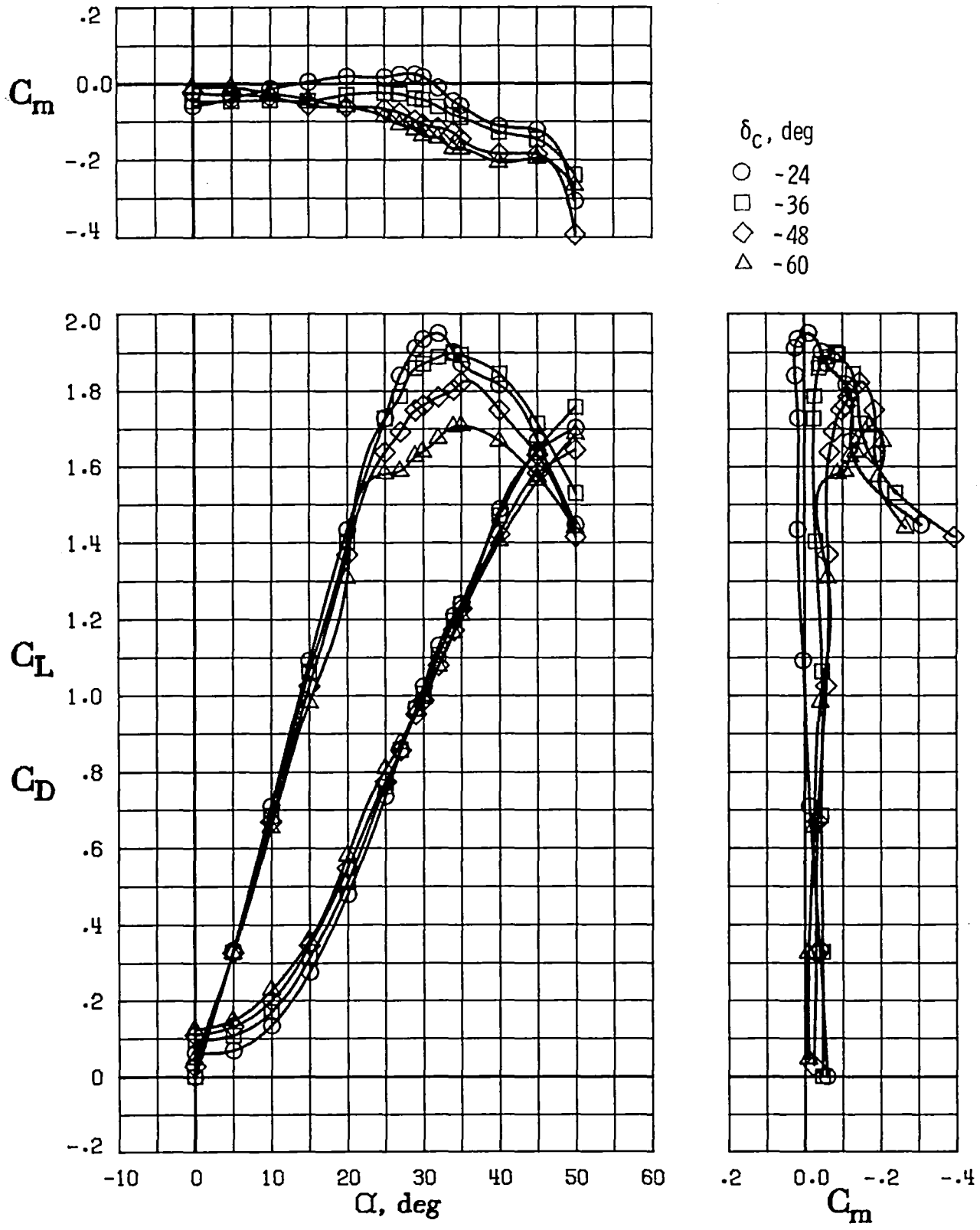

(b) Large deflections.

Figure 8.- Concluded.

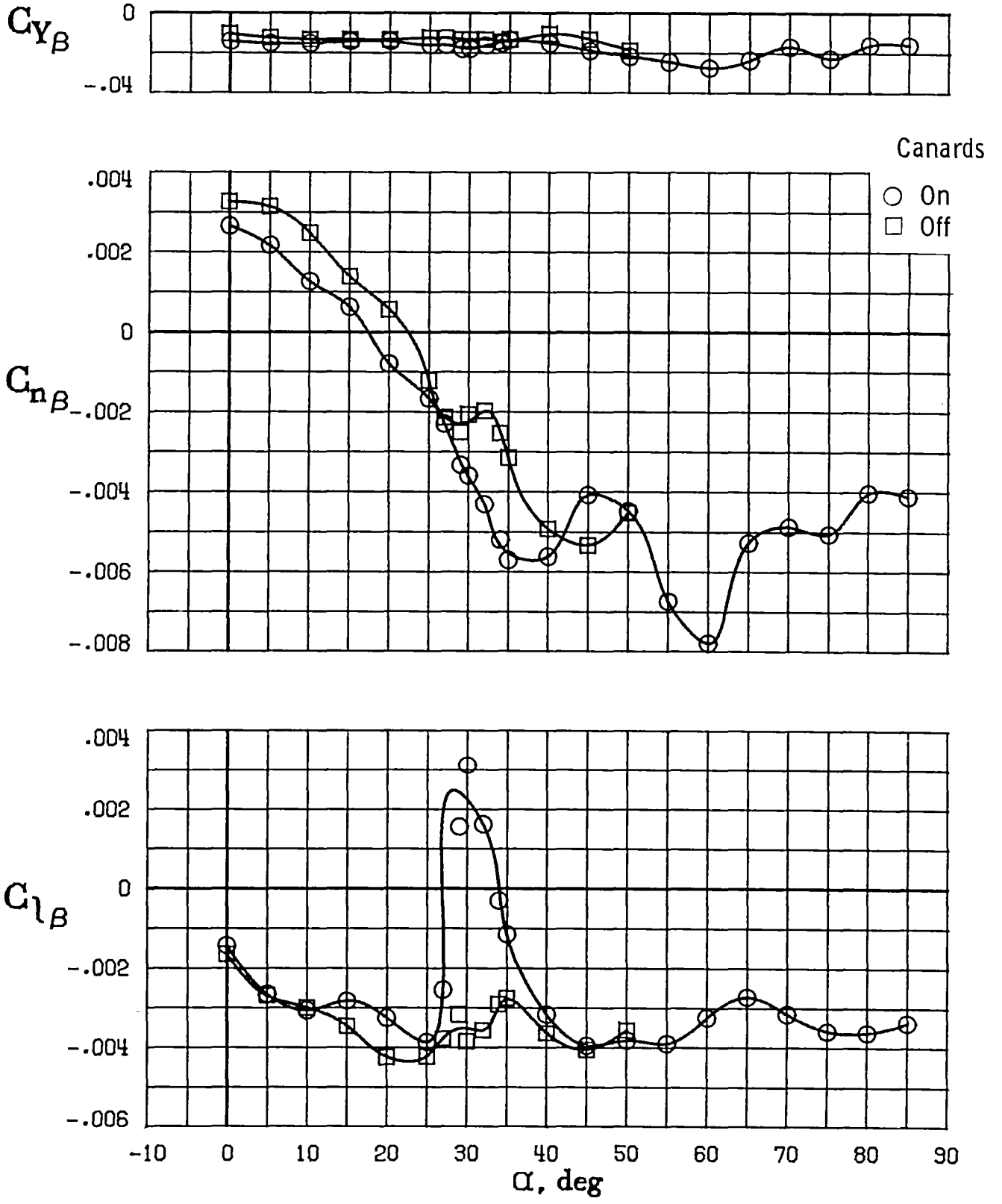

Figure 9.- Effect of canards on static lateral-directional characteristics.

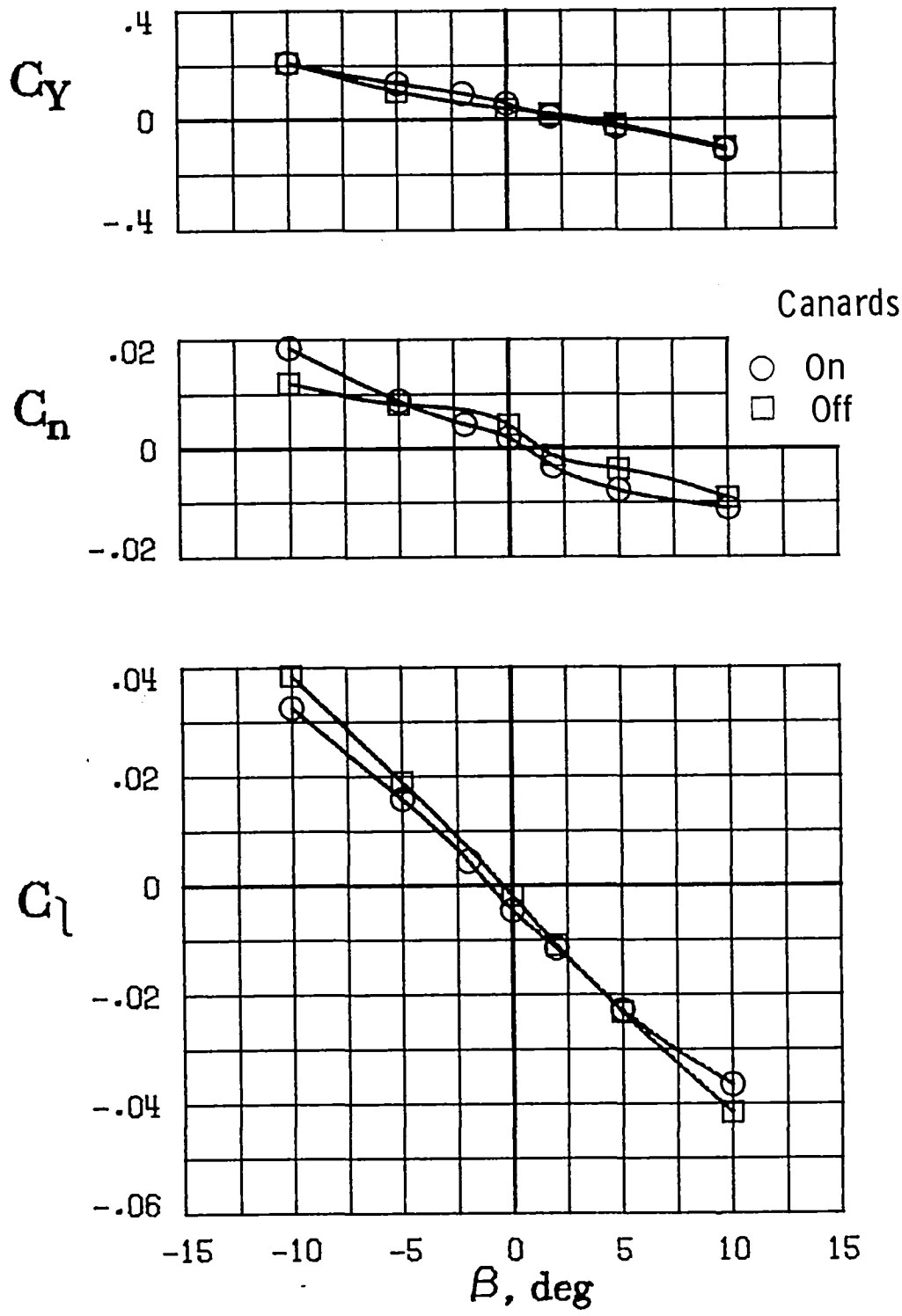

(a) $\alpha = 25°$.

Figure 10.- Effect of canards on static lateral-directional characteristics with sideslip angle. $\delta_c = 0°$.

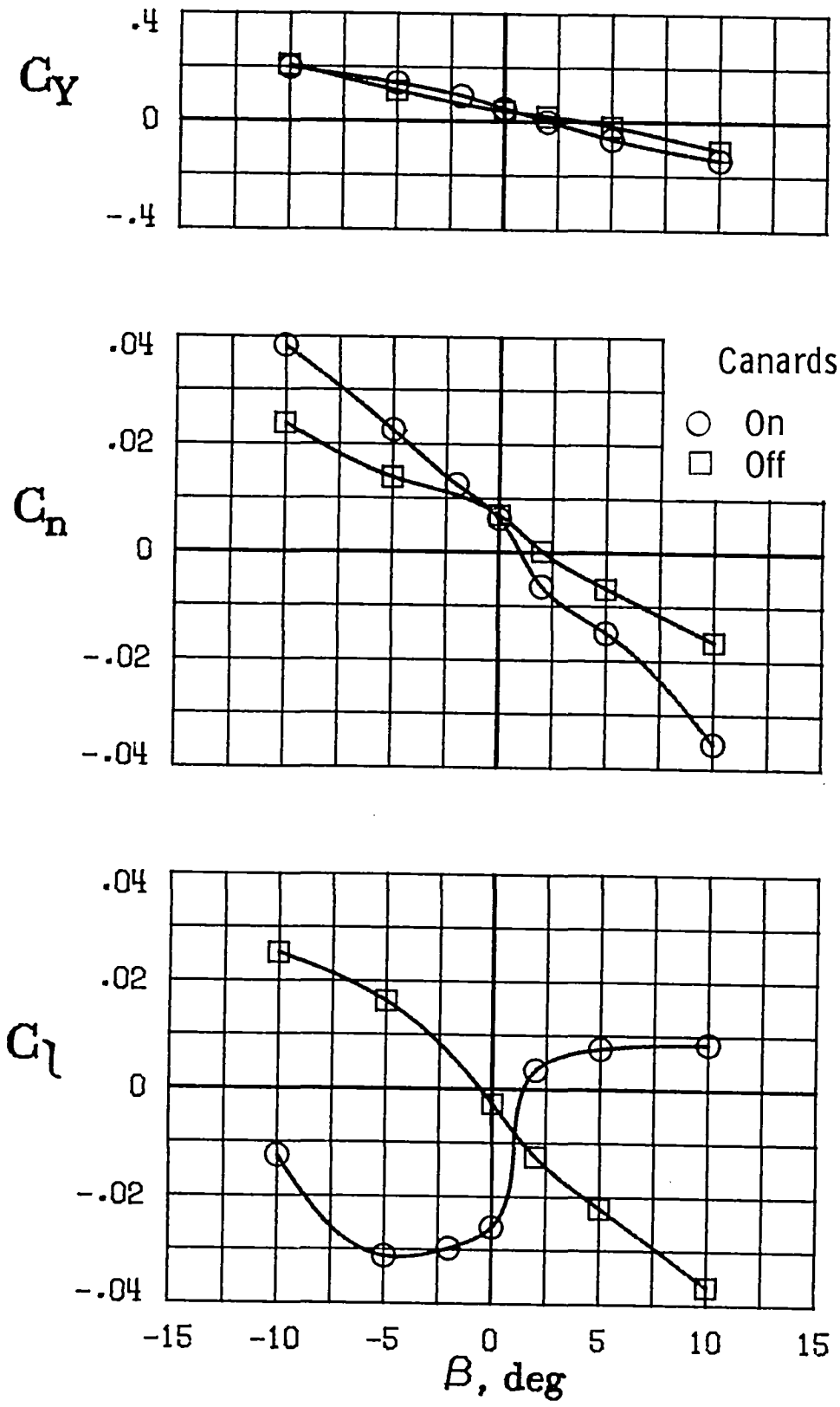

(b) $\alpha = 30°$.

Figure 10.- Continued.

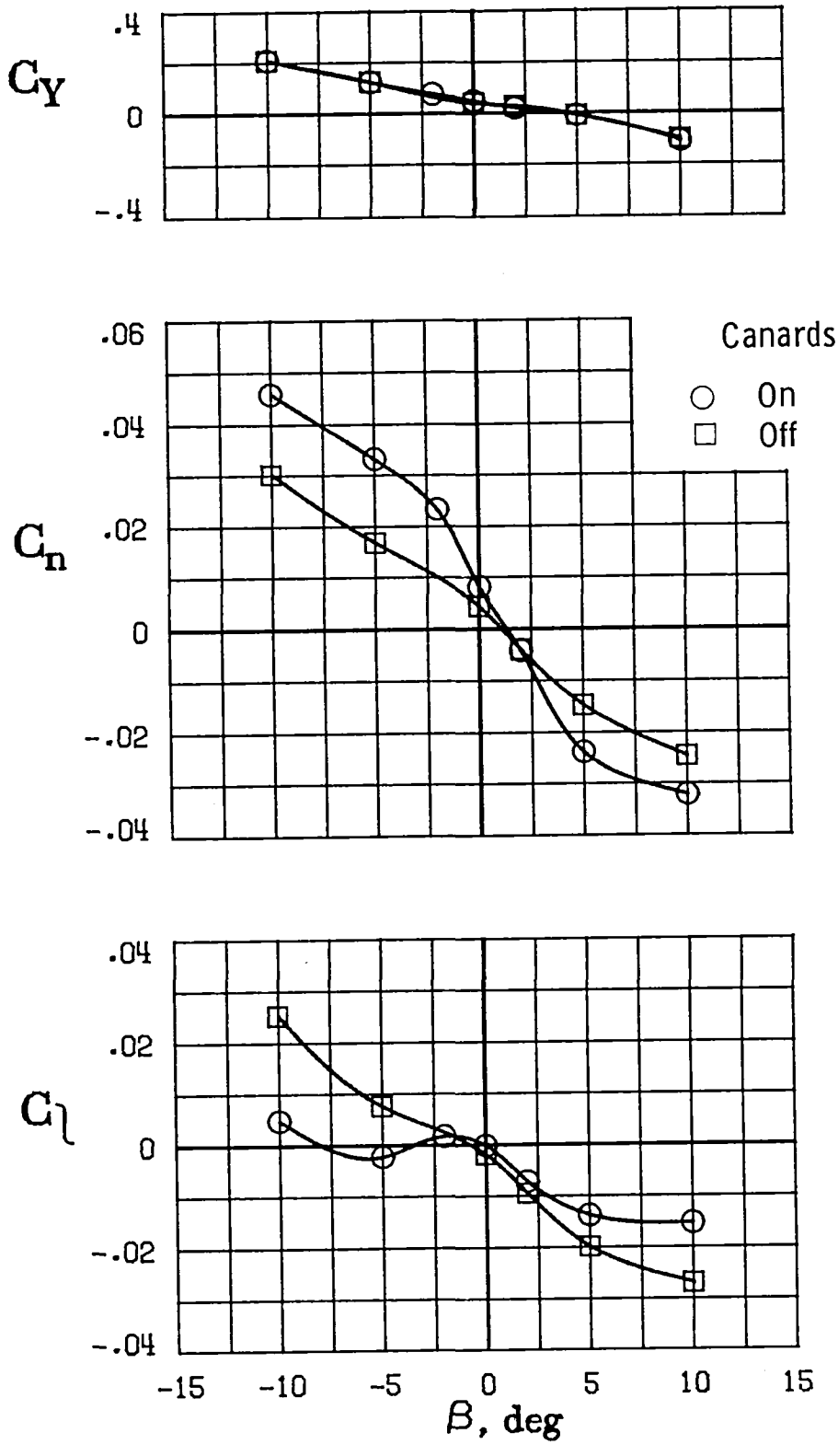

(c) $\alpha = 35°$.

Figure 10.- Concluded.

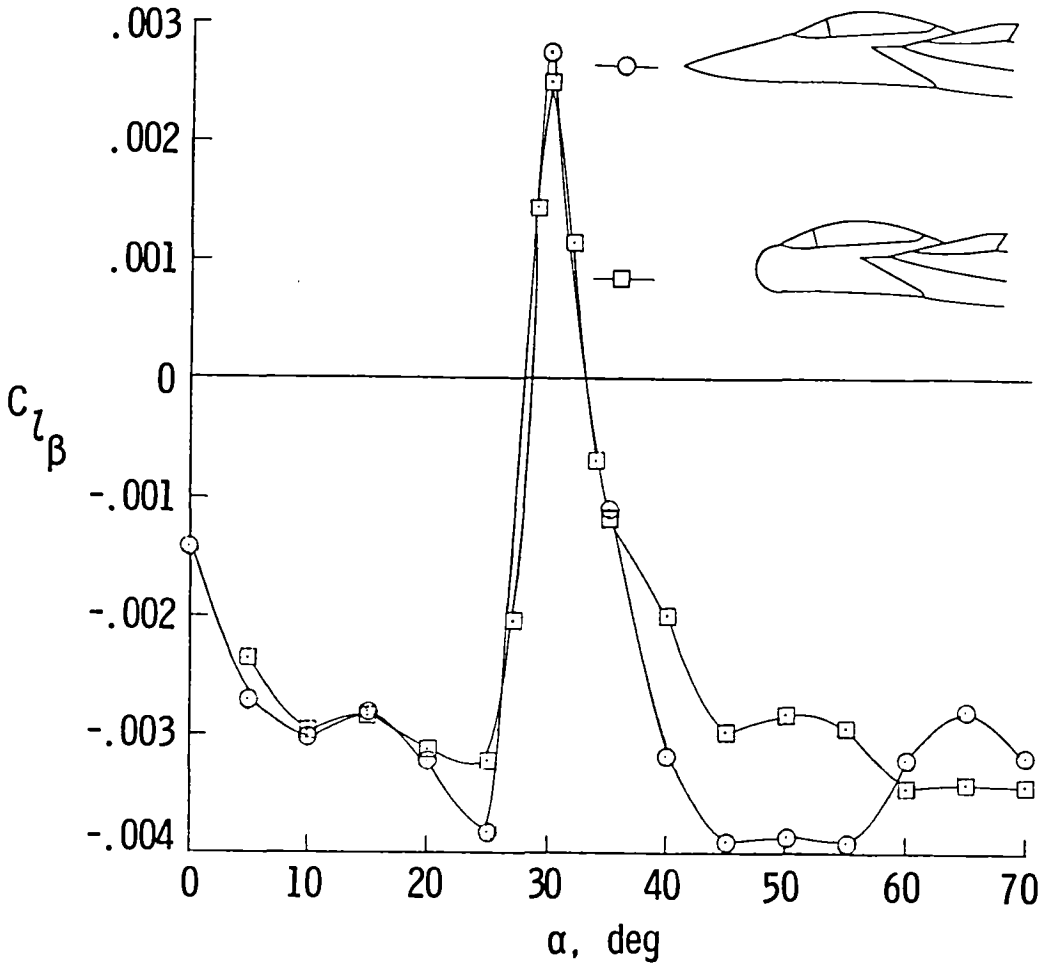

Figure 11.- Influence of nose shape on static lateral stability.

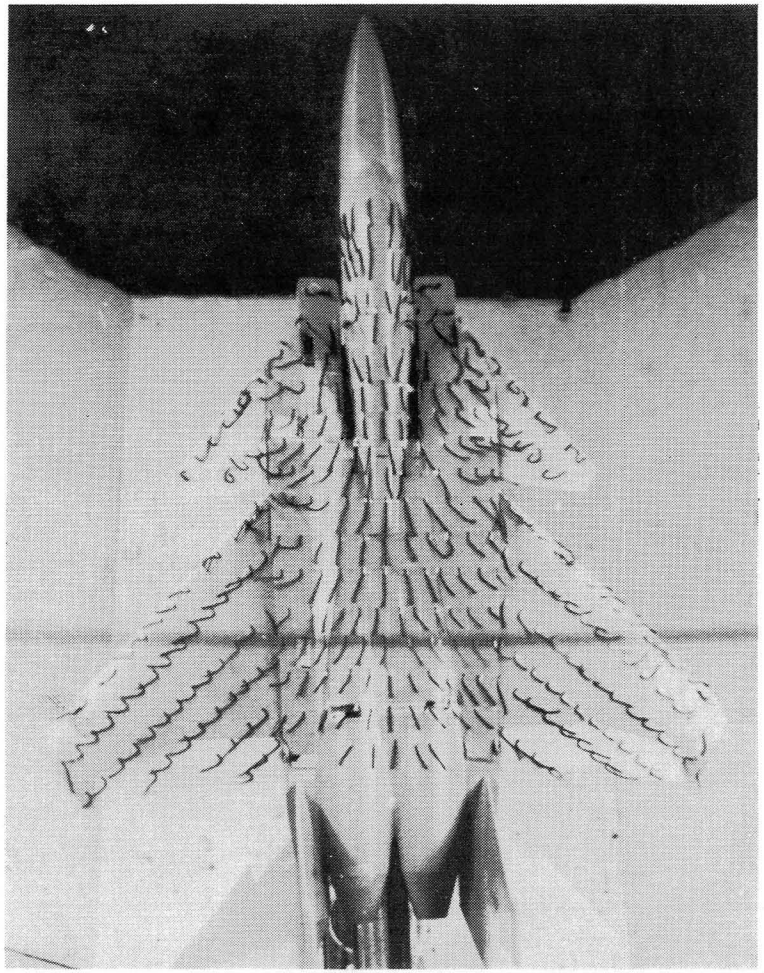

$\beta = 0°$

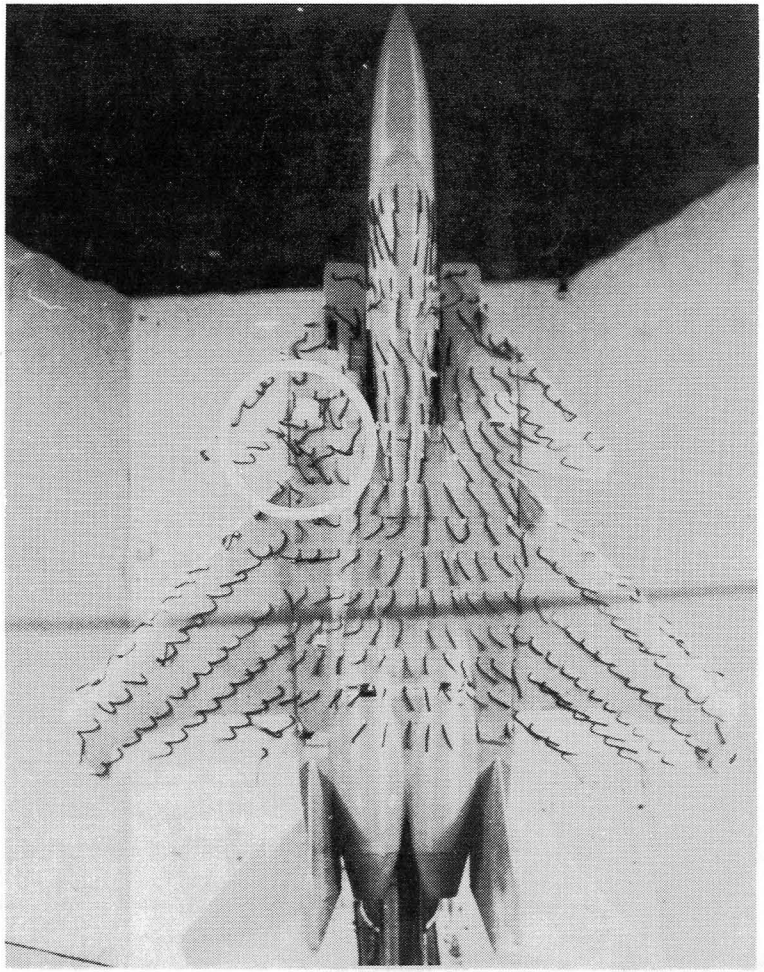

$\beta = -5°$

L-83-07

Figure 12.- Surface flow visualization at $\alpha = 30°$.

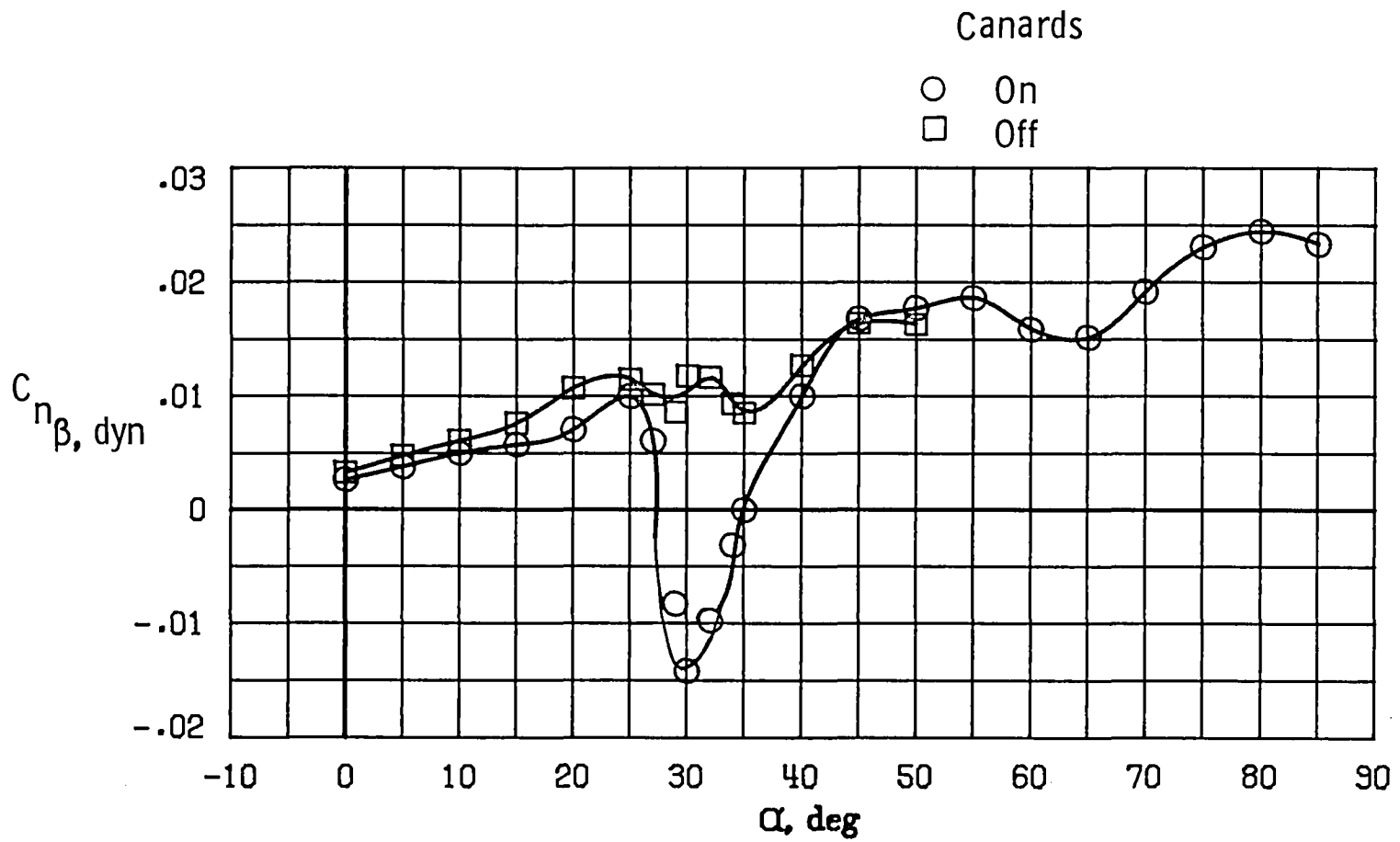

Figure 13.- Effect of canards on variation of $C_{n_{\beta,dyn}}$ with angle of attack.

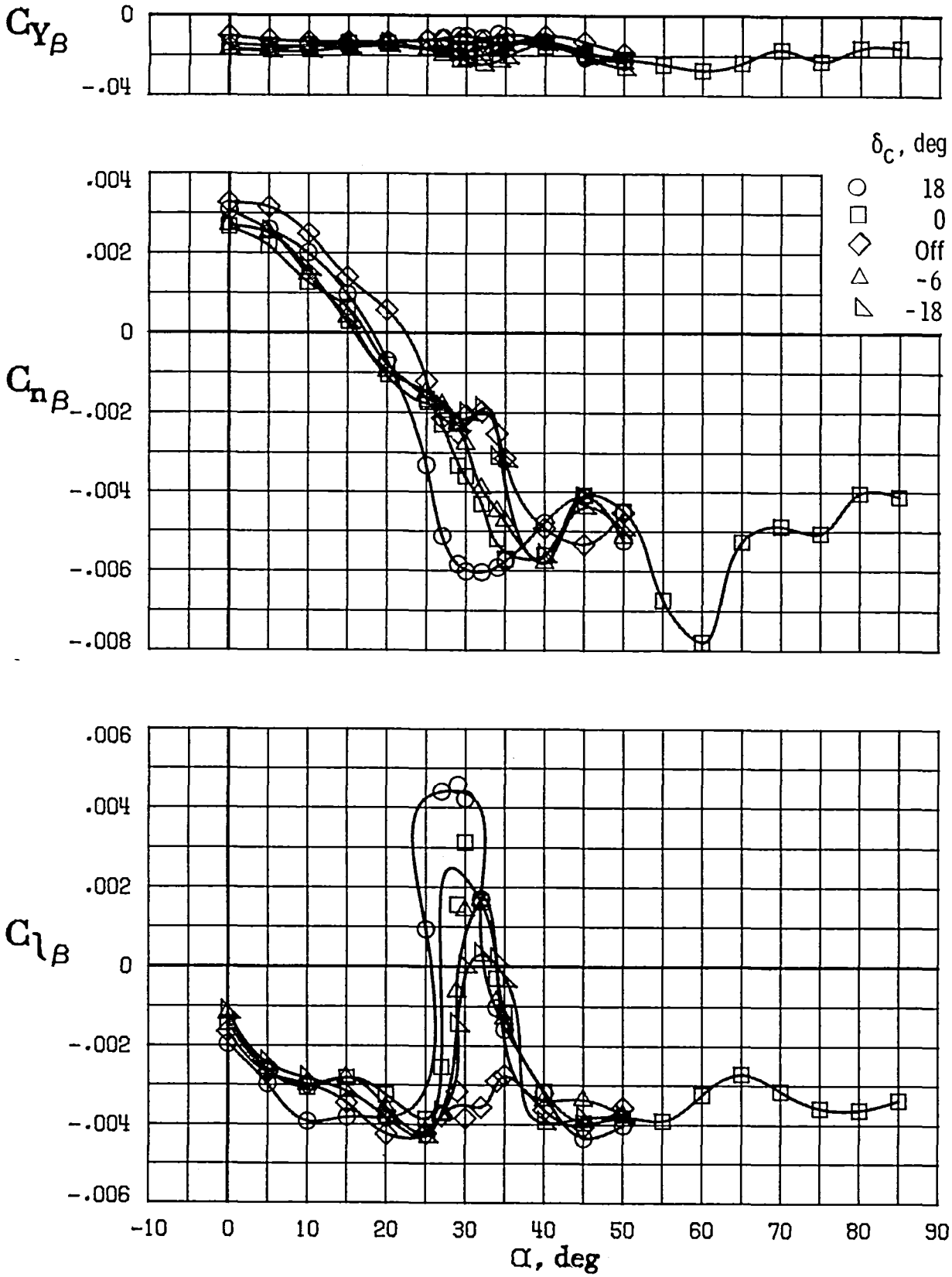

(a) Moderate deflections.

Figure 14.- Effect of canard deflection on static lateral-directional characteristics.

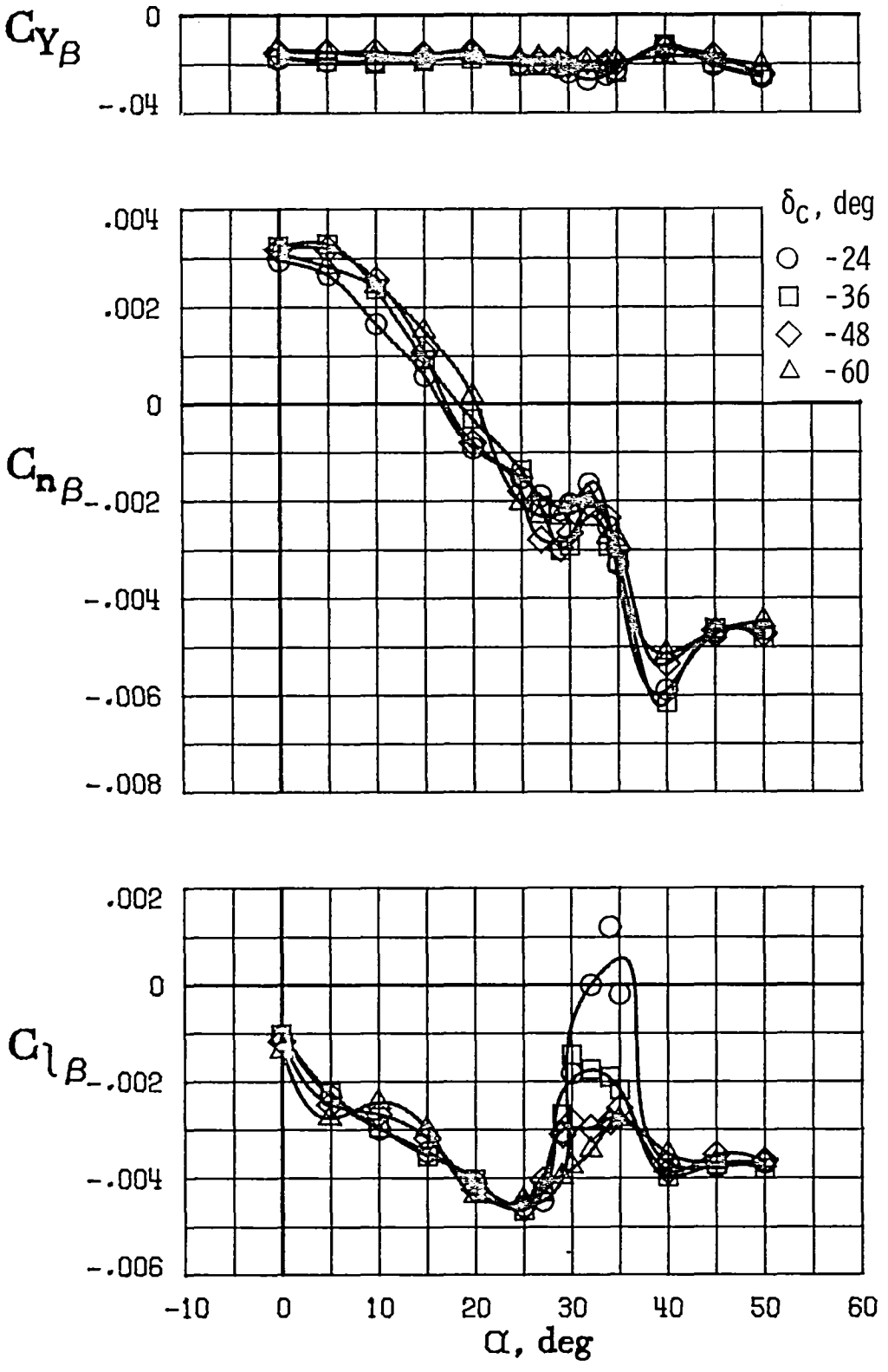

(b) Large deflections.

Figure 14.- Concluded.

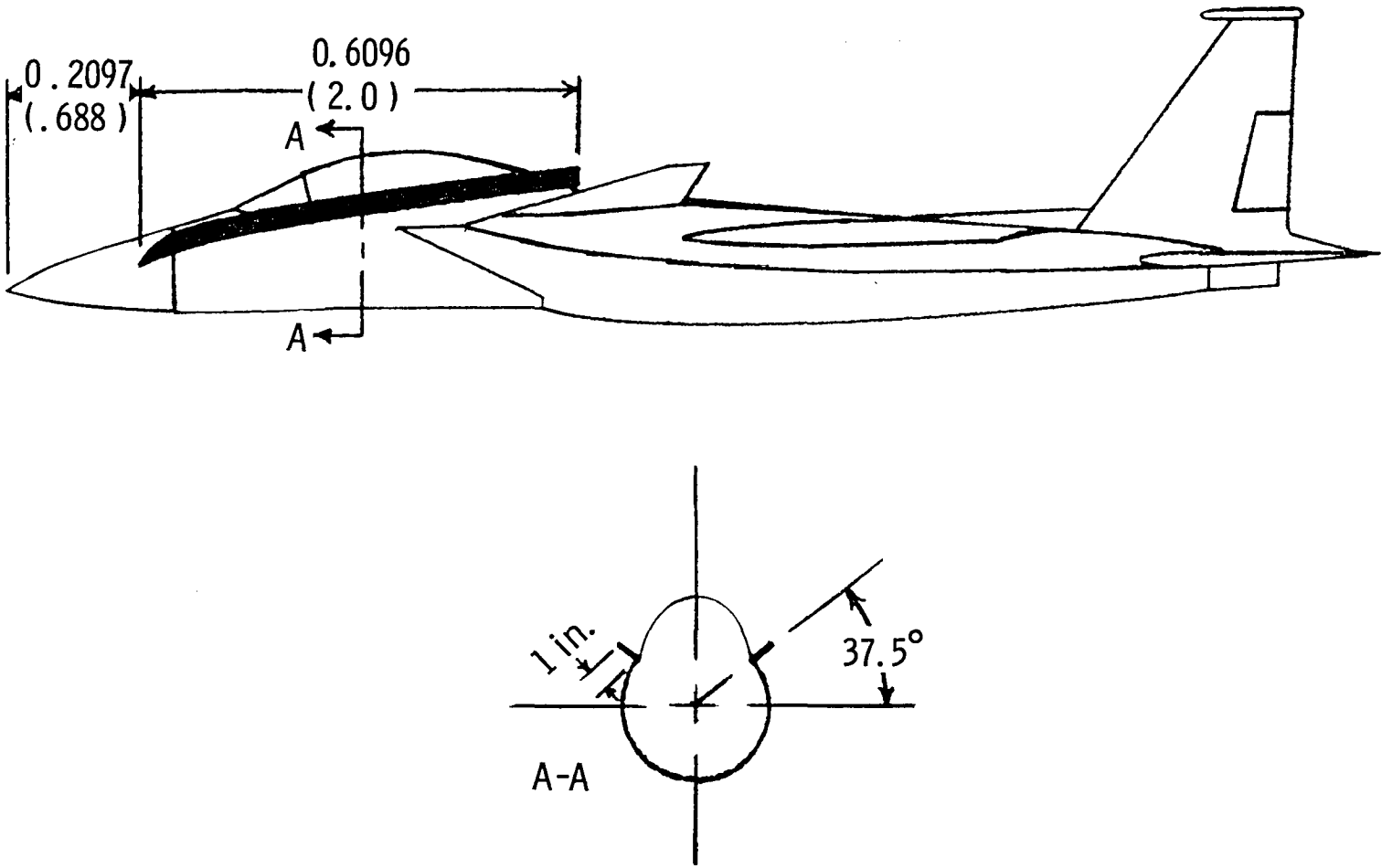

Figure 15.- Side view and cross section of fuselage strake. Dimensions are given in meters (feet) unless otherwise indicated.

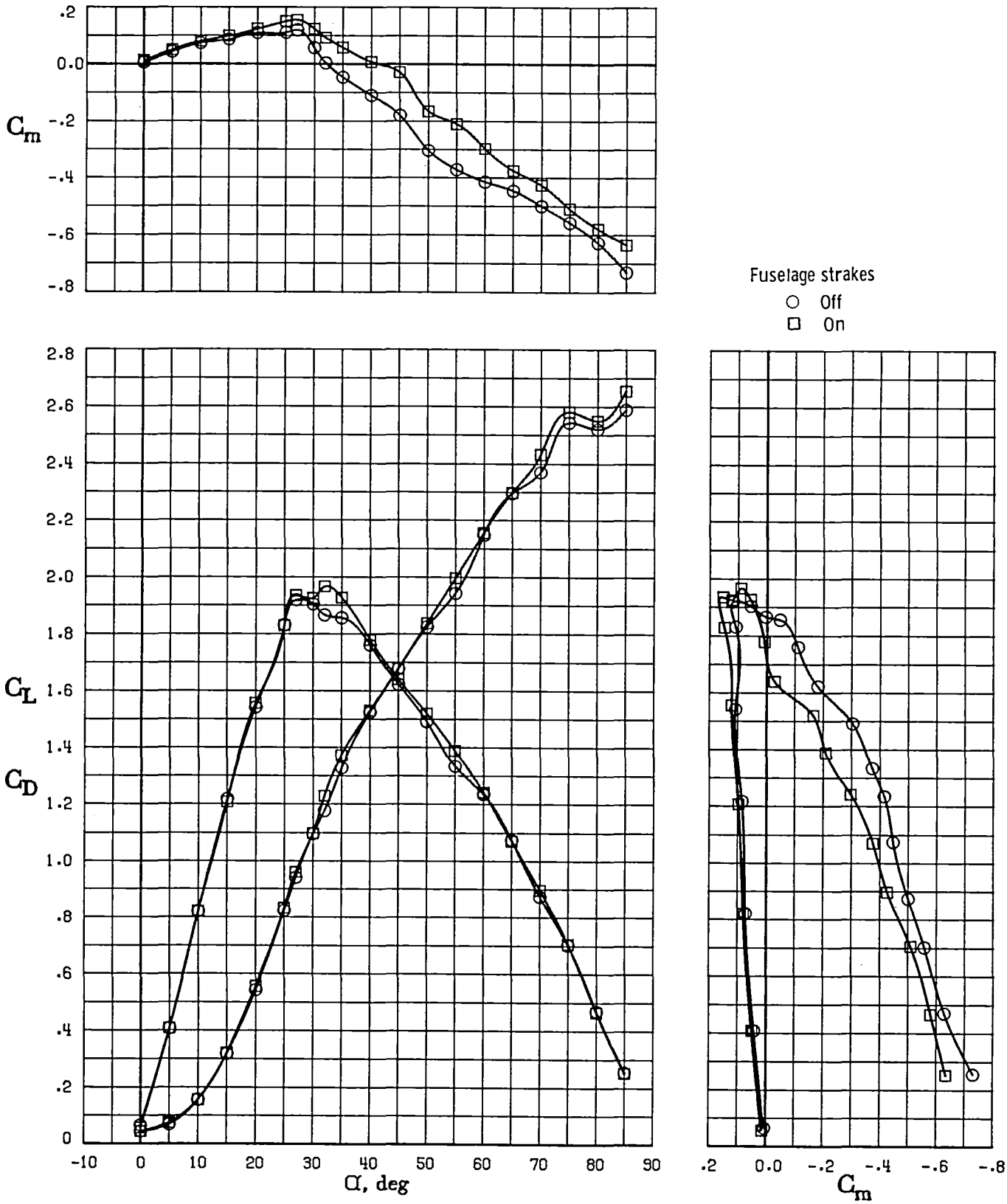

Figure 16.- Effect of fuselage strakes on longitudinal characteristics. $\delta_c = 0°$.

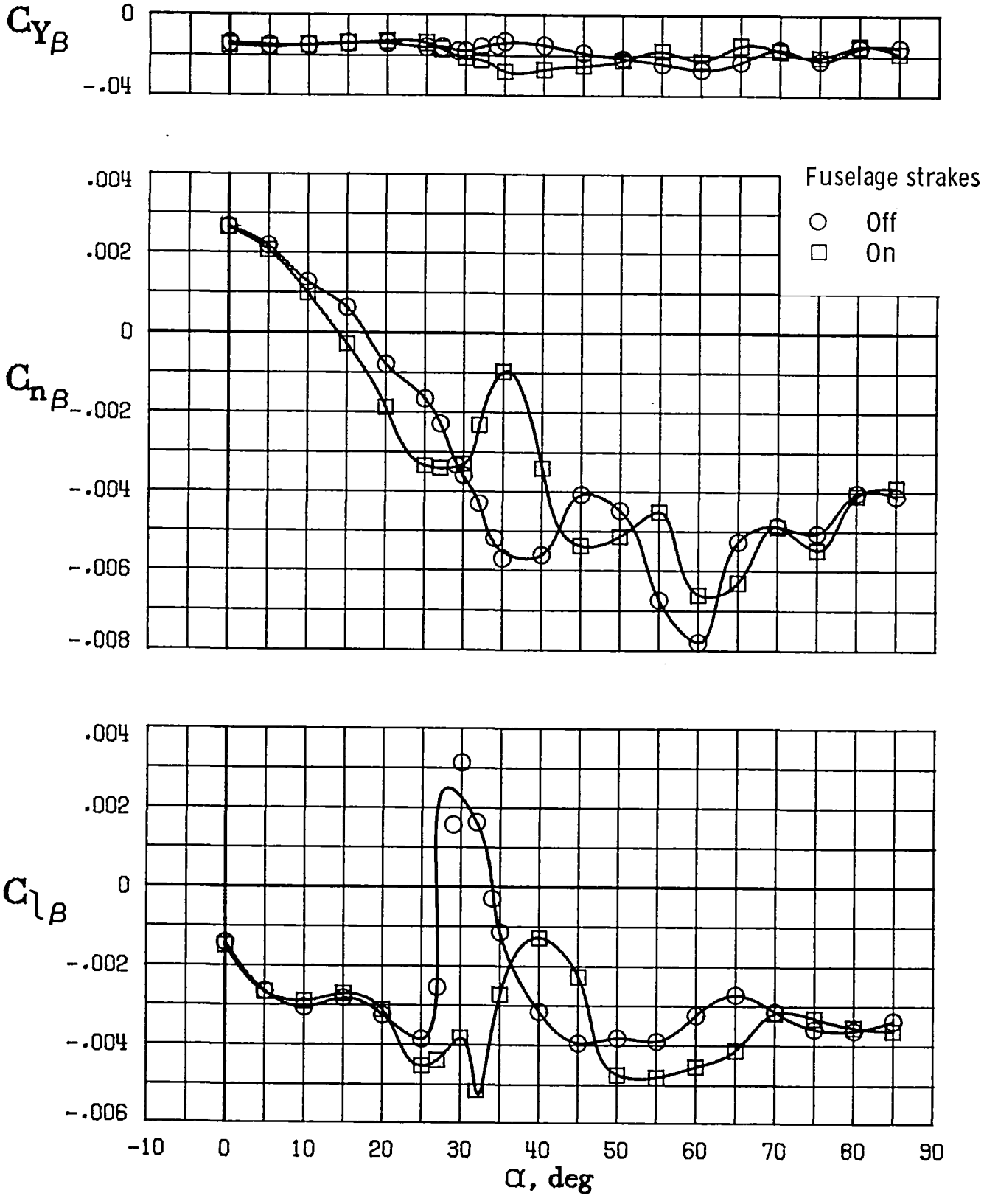

Figure 17.- Effect of fuselage strakes on lateral-directional characteristics. $\delta_c = 0°$.

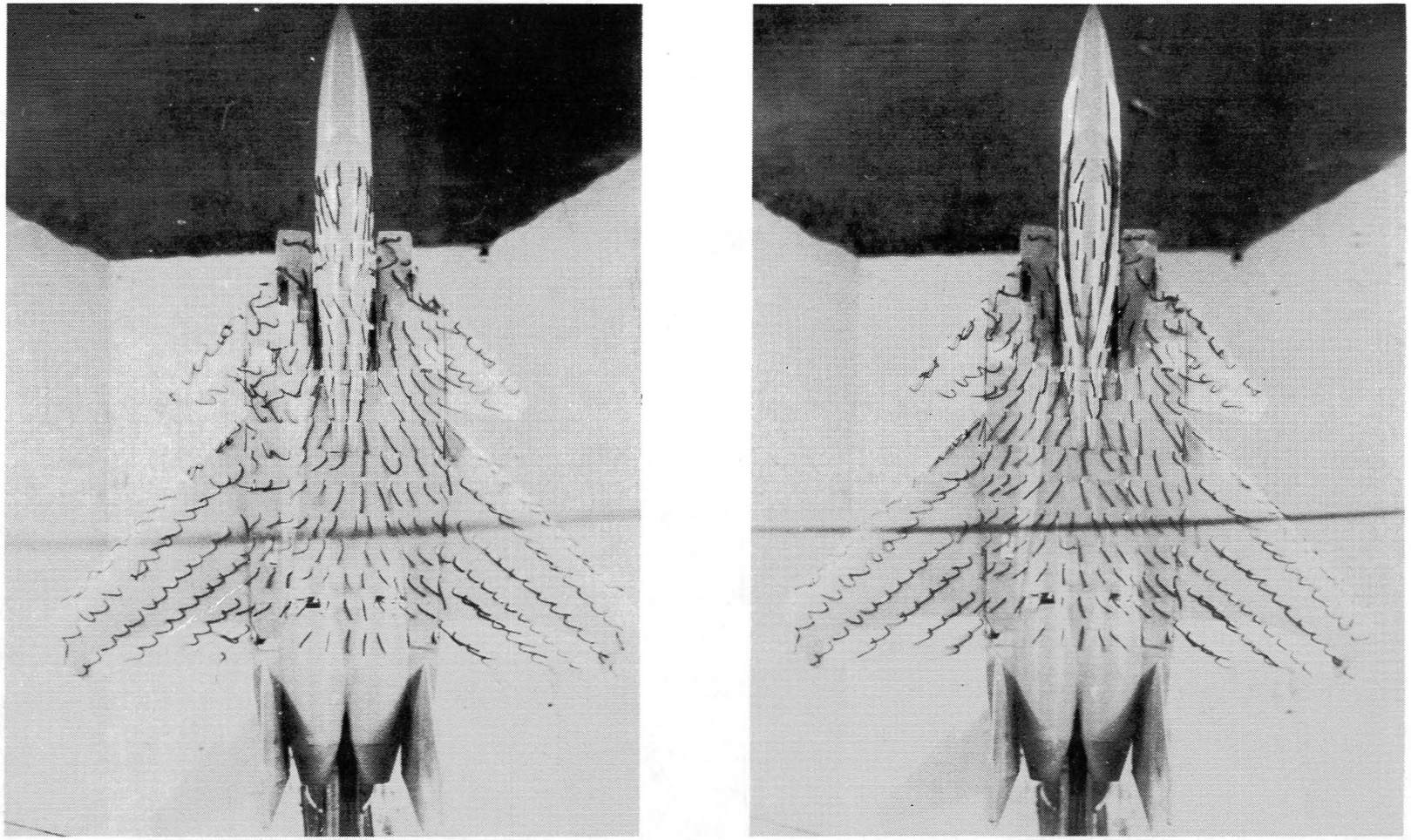

Strake off

Strake on

L-83-08

Figure 18.- Effect of strake on surface flow visualization at $\alpha = 30°$, $\beta = -5°$.

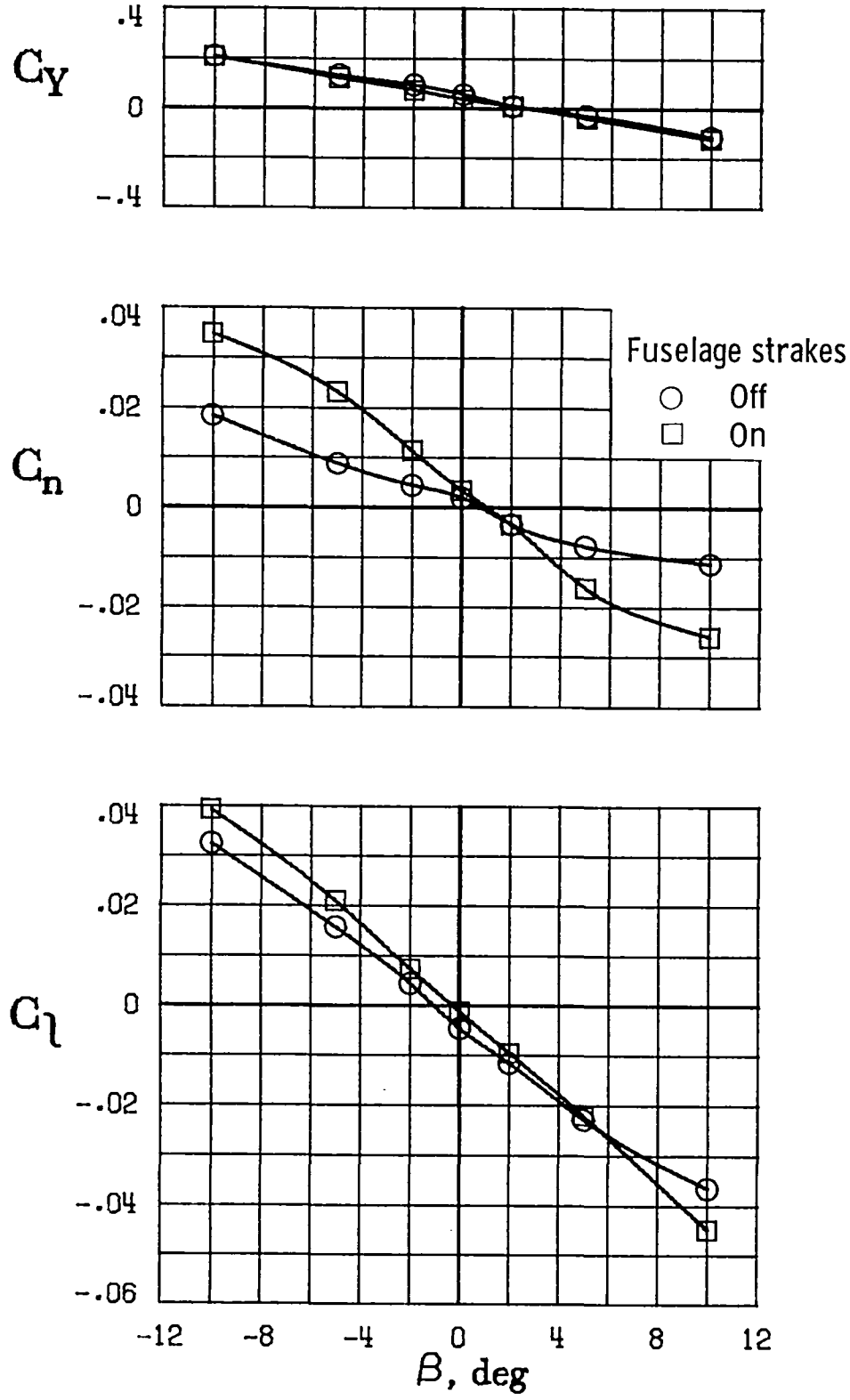

(a) $\alpha = 25°$.

Figure 19.- Effect of fuselage strakes on static lateral-directional characteristics with sideslip angle. $\delta_c = 0°$.

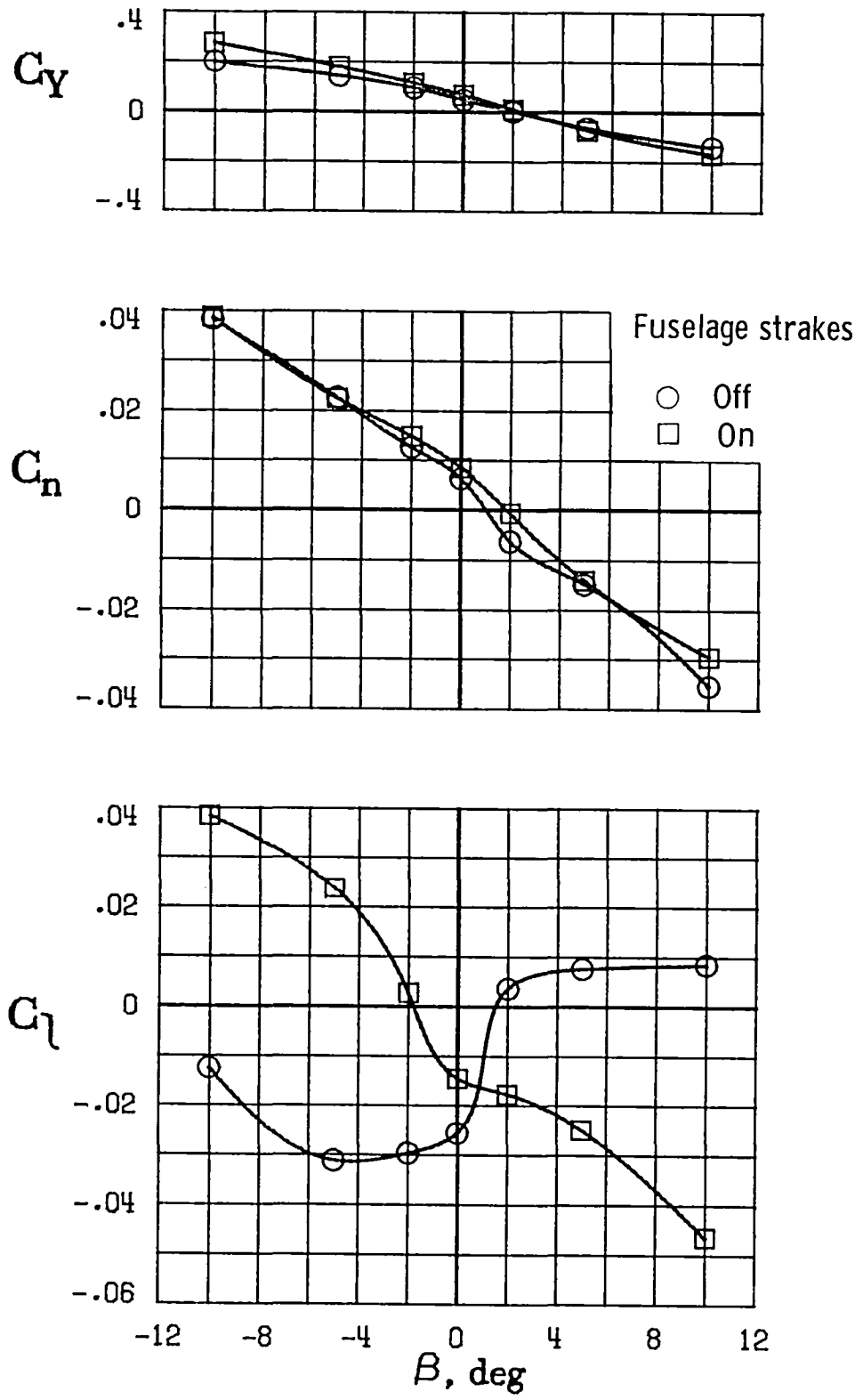

(b) $\alpha = 30°$.

Figure 19.- Continued.

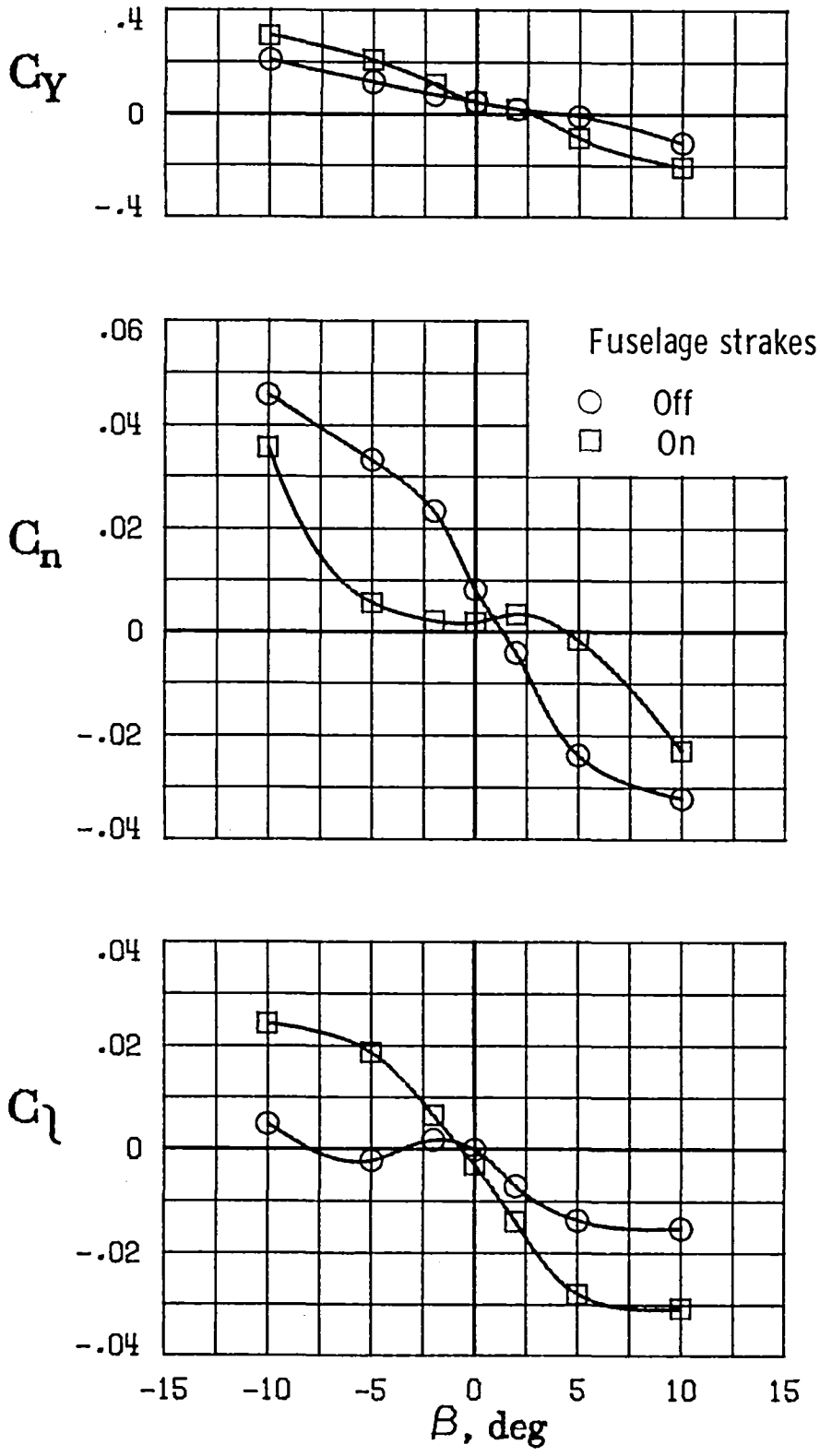

(c) $\alpha = 35°$.

Figure 19.- Concluded.

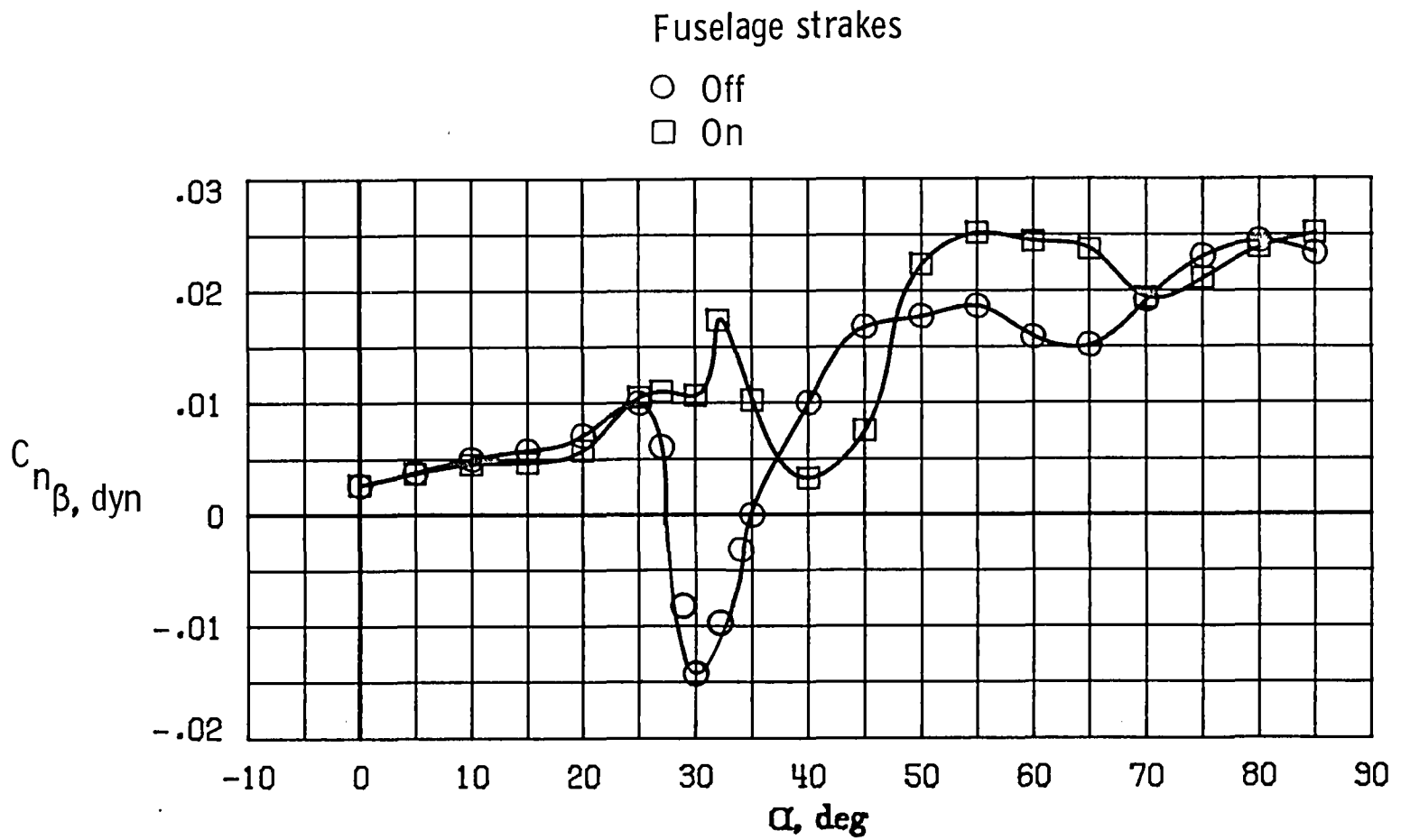

Figure 20.- Effect of fuselage strakes on variation of $C_{n_{\beta,dyn}}$ with angle of attack.

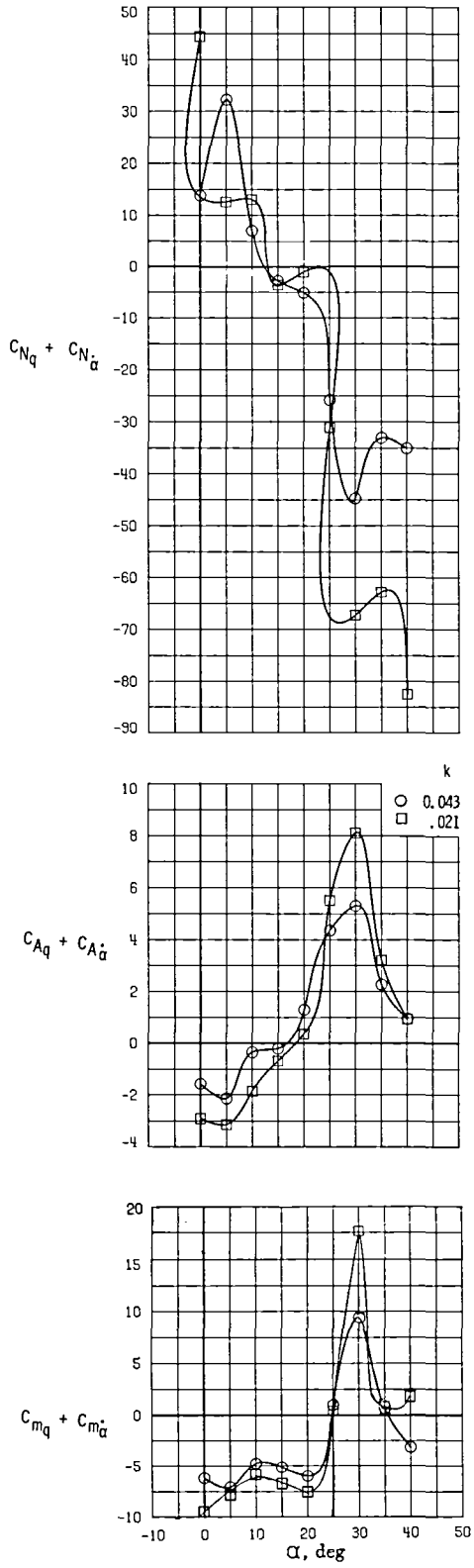

Figure 21.- Effect of frequency on dynamic pitching derivatives. $\delta_h = 0°$; $\Delta\theta = \pm 5°$; $\delta_c = 0°$.

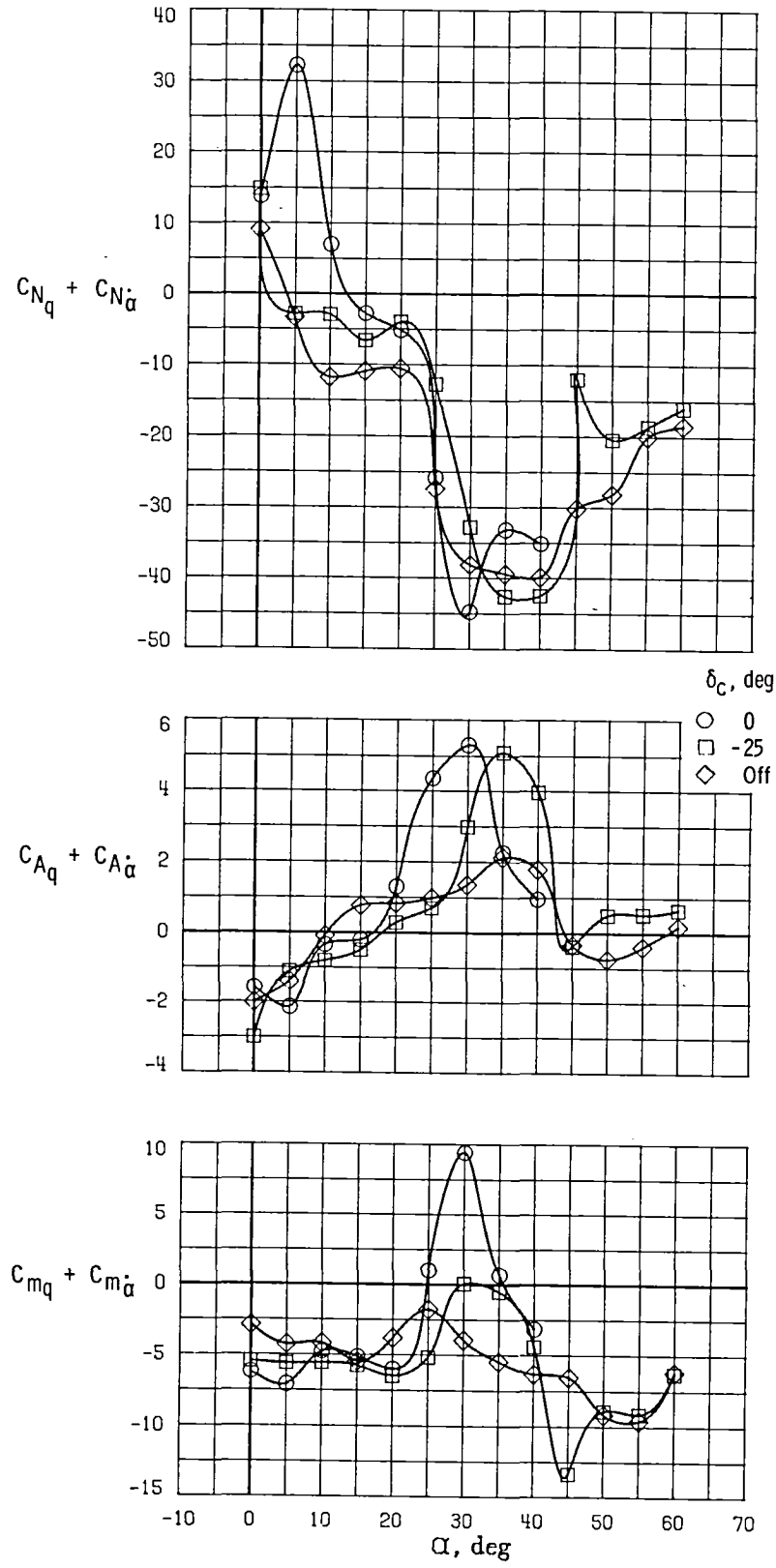

Figure 22.- Effect of canards on dynamic pitching derivatives. $\delta_h = 0°$; $\Delta\theta = \pm 5°$; $k = 0.043$.

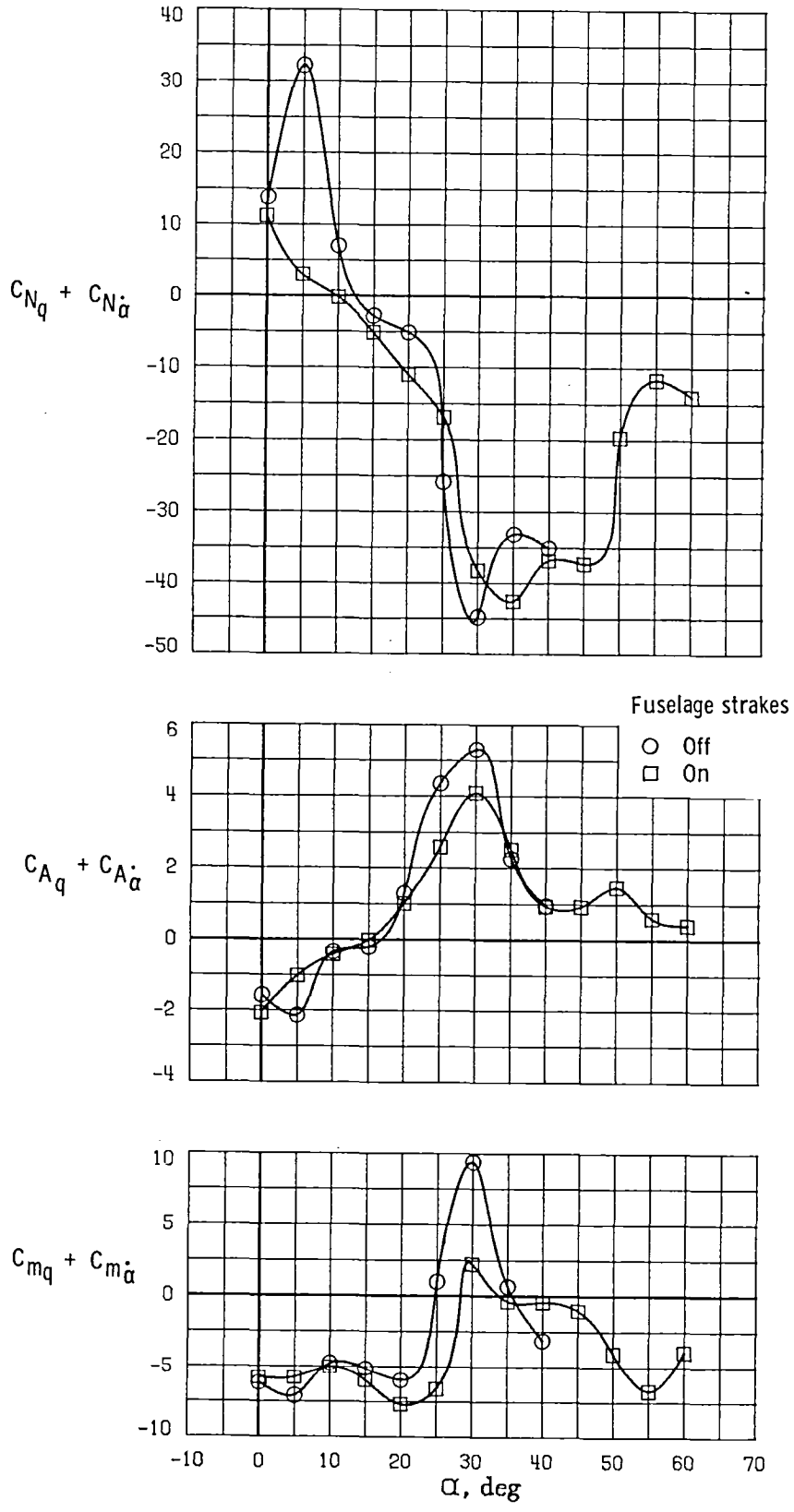

Figure 23.- Effect of fuselage strakes on dynamic pitching derivatives. $k = 0.043$; $\delta_h = 0°$; $\Delta\theta = \pm 5°$; $\delta_c = 0°$.

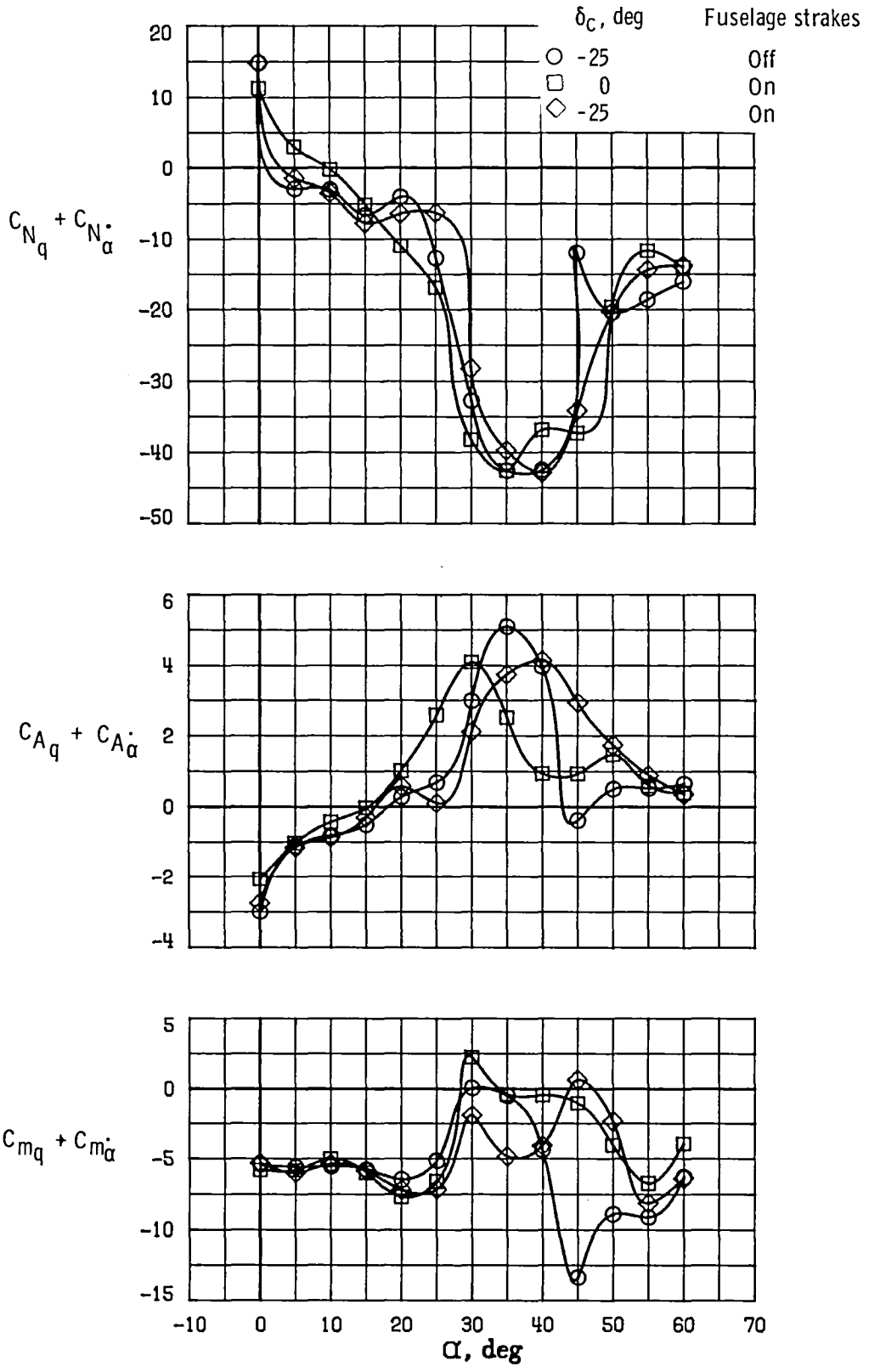

Figure 24.- Effect of canard deflection and fuselage strakes on dynamic pitching derivatives. k = 0.043; δ_h = 0°; Δθ = ±5°.

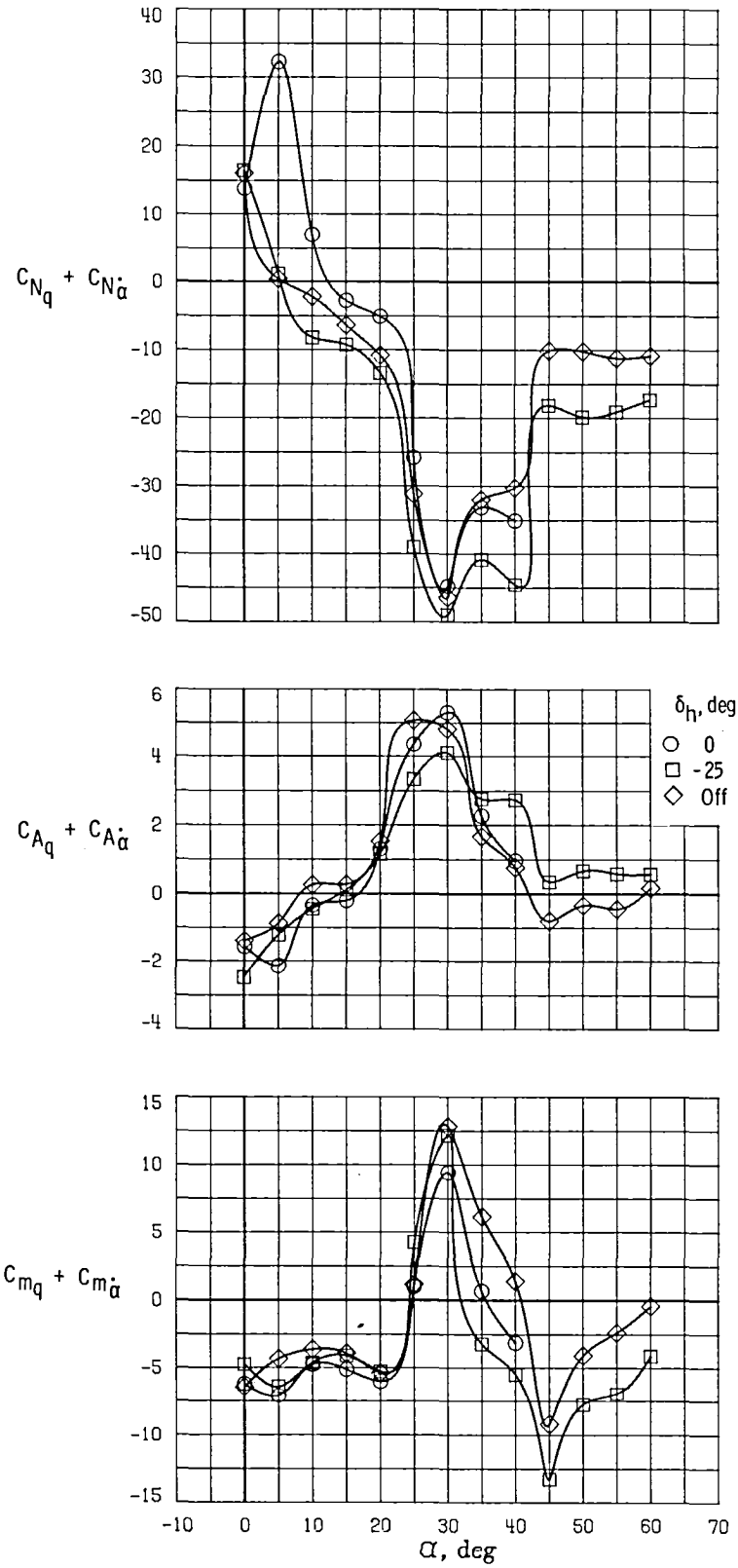

Figure 25.- Effect of horizontal tails on dynamic pitching derivatives. $\delta_c = 0°$; $\Delta\theta = \pm 5°$; $k = 0.043$.

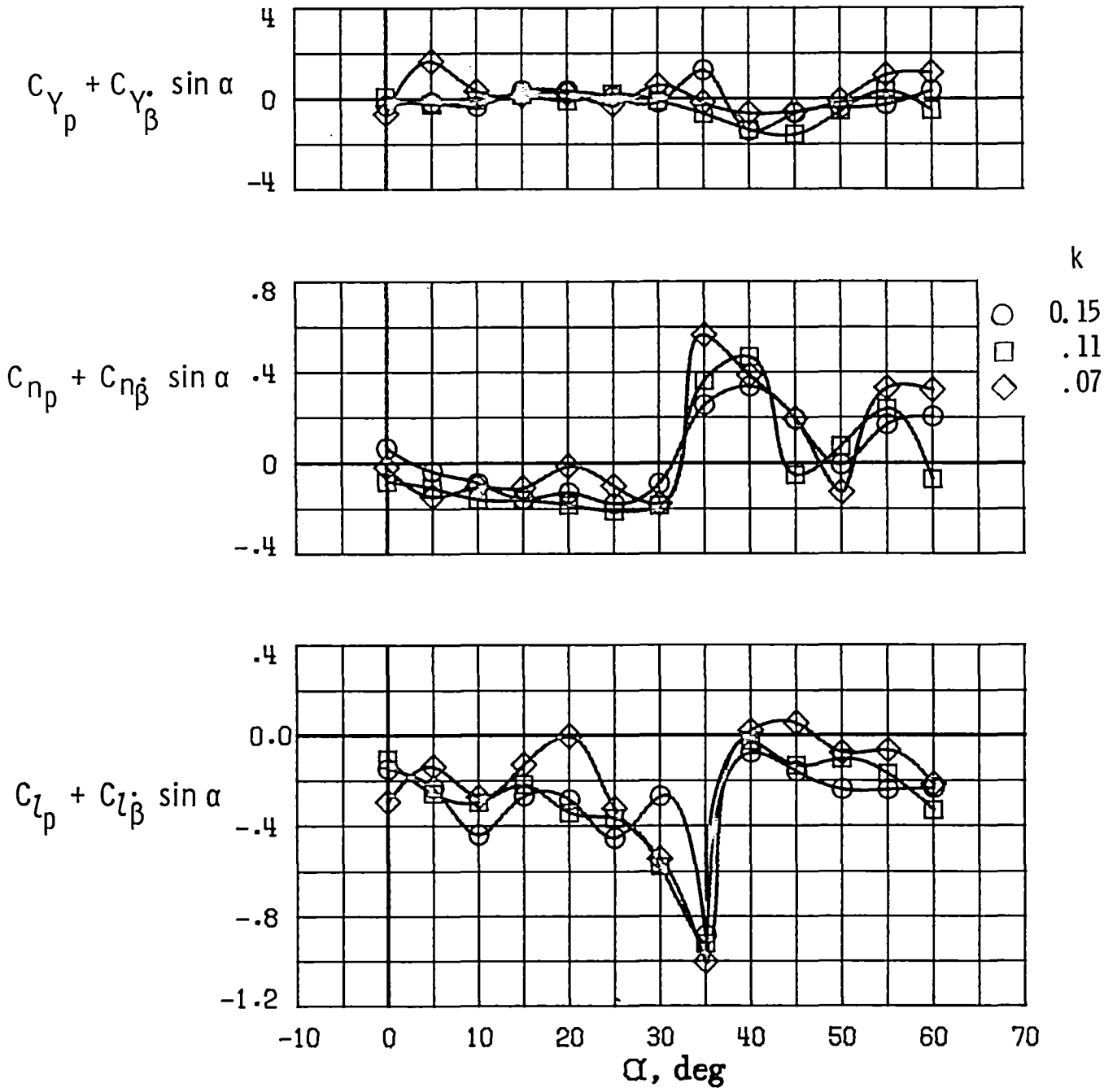

Figure 26.- Effect of frequency on dynamic rolling derivatives. $\Delta\phi = \pm 5°$; $\delta_c = 0°$.

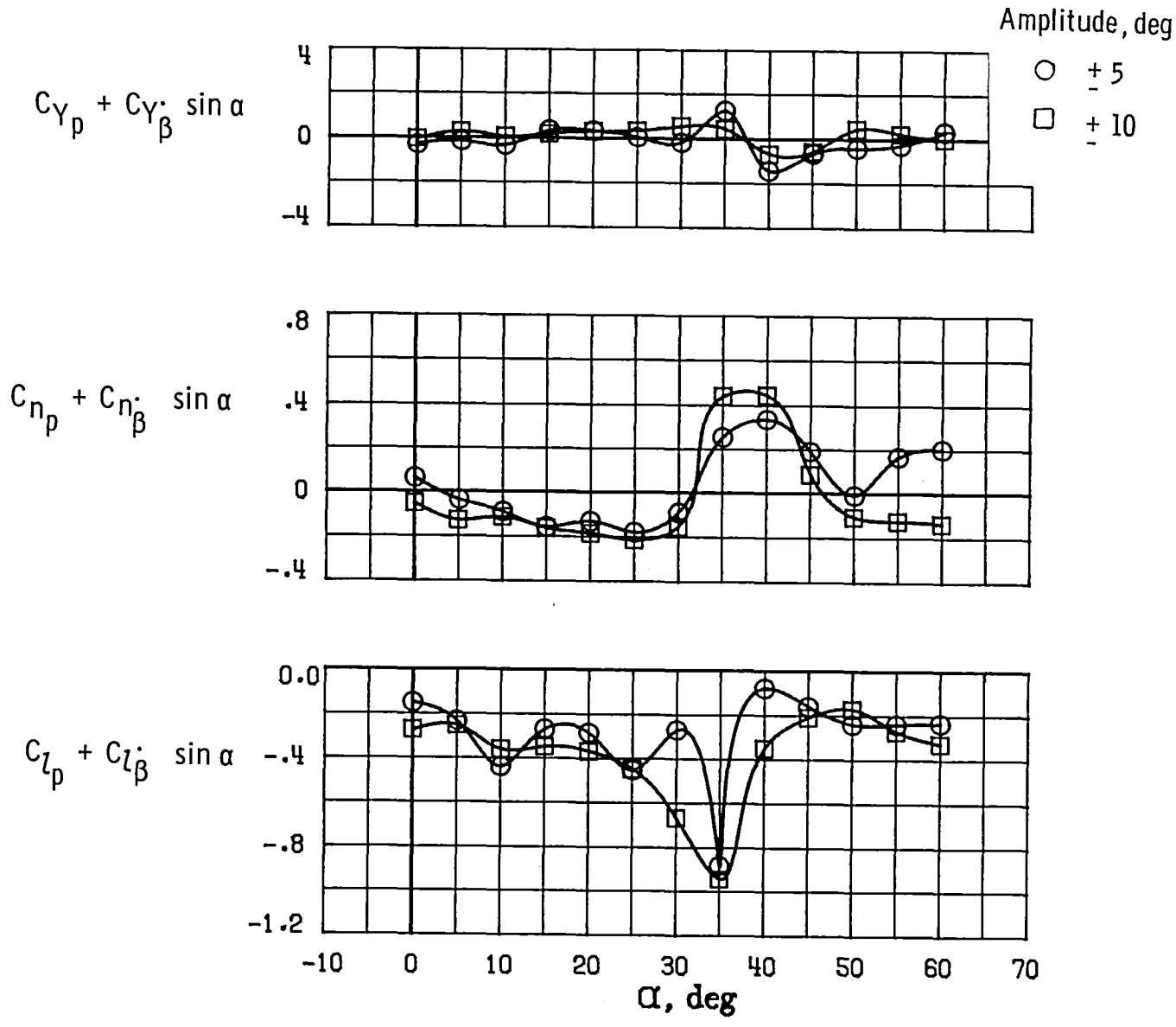

Figure 27.- Effect of amplitude on dynamic rolling derivatives. k = 0.15; $\delta_c = 0°$; $\delta_h = 0°$.

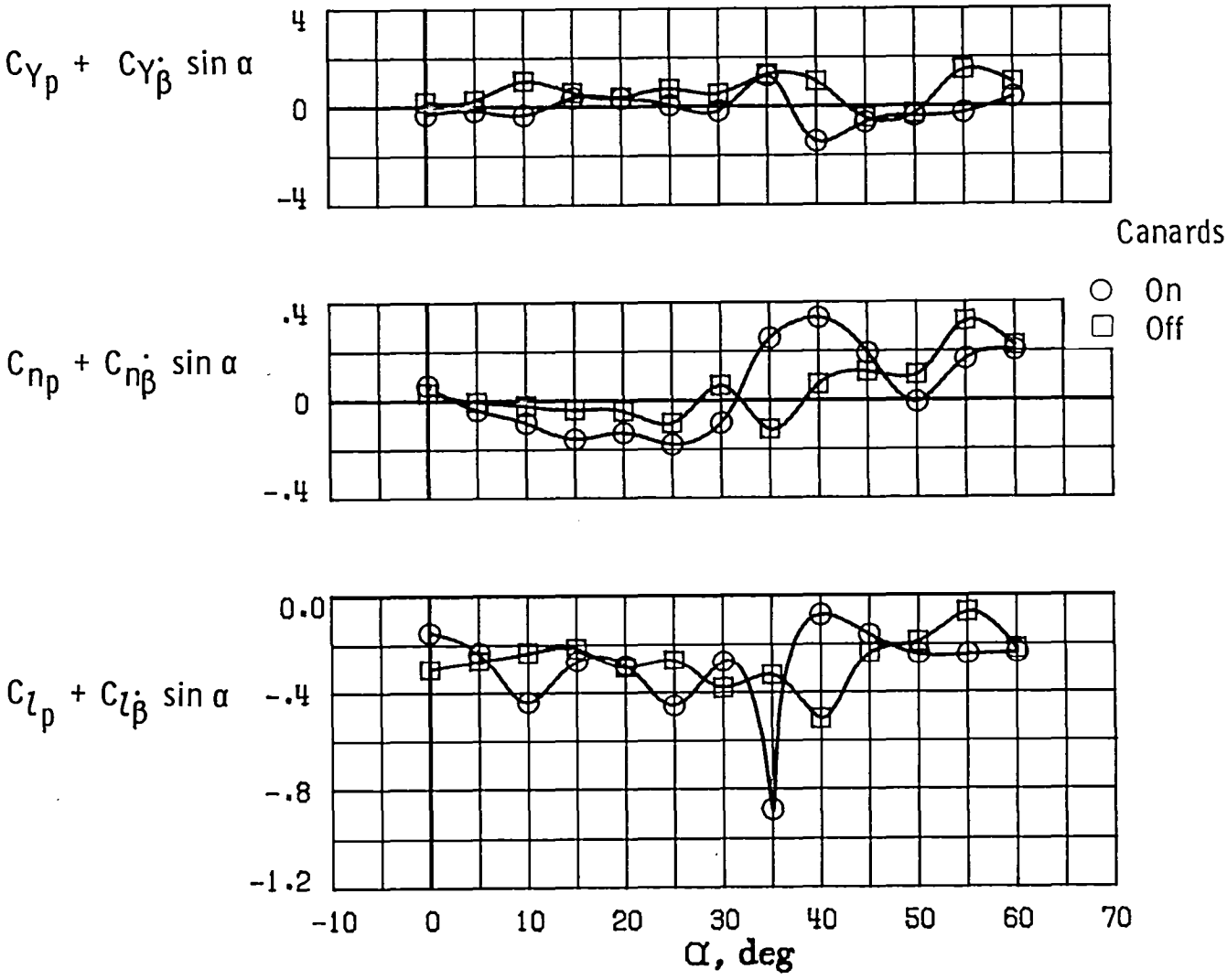

Figure 28.- Effect of canards on dynamic rolling derivatives. $\Delta\phi = \pm 5°$; $\delta_h = 0°$; $k = 0.15$; $\delta_c = 0°$.

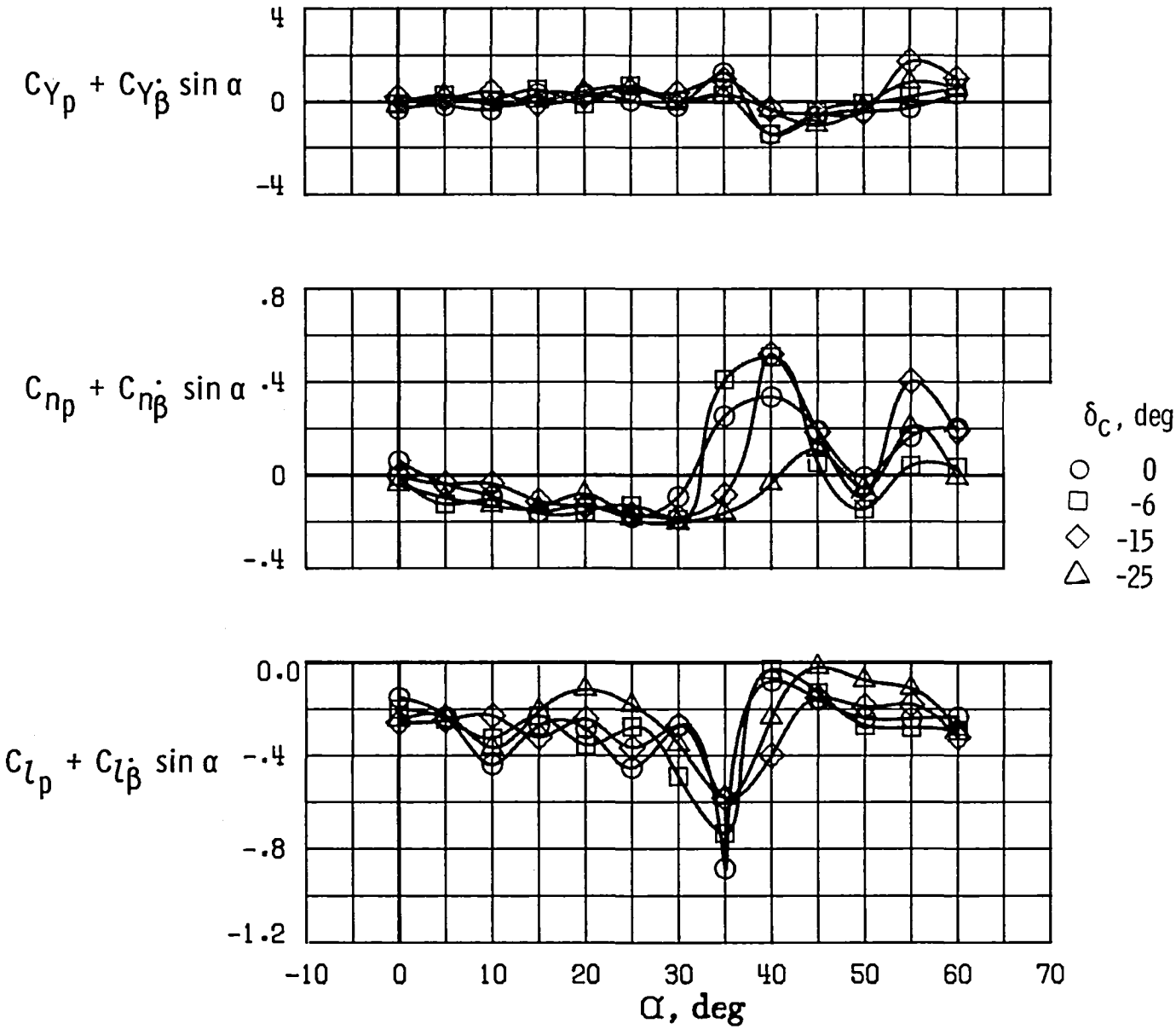

Figure 29.- Effect of canard deflection on dynamic rolling derivatives. $\Delta\phi = \pm 5°$; $\delta_h = 0°$.

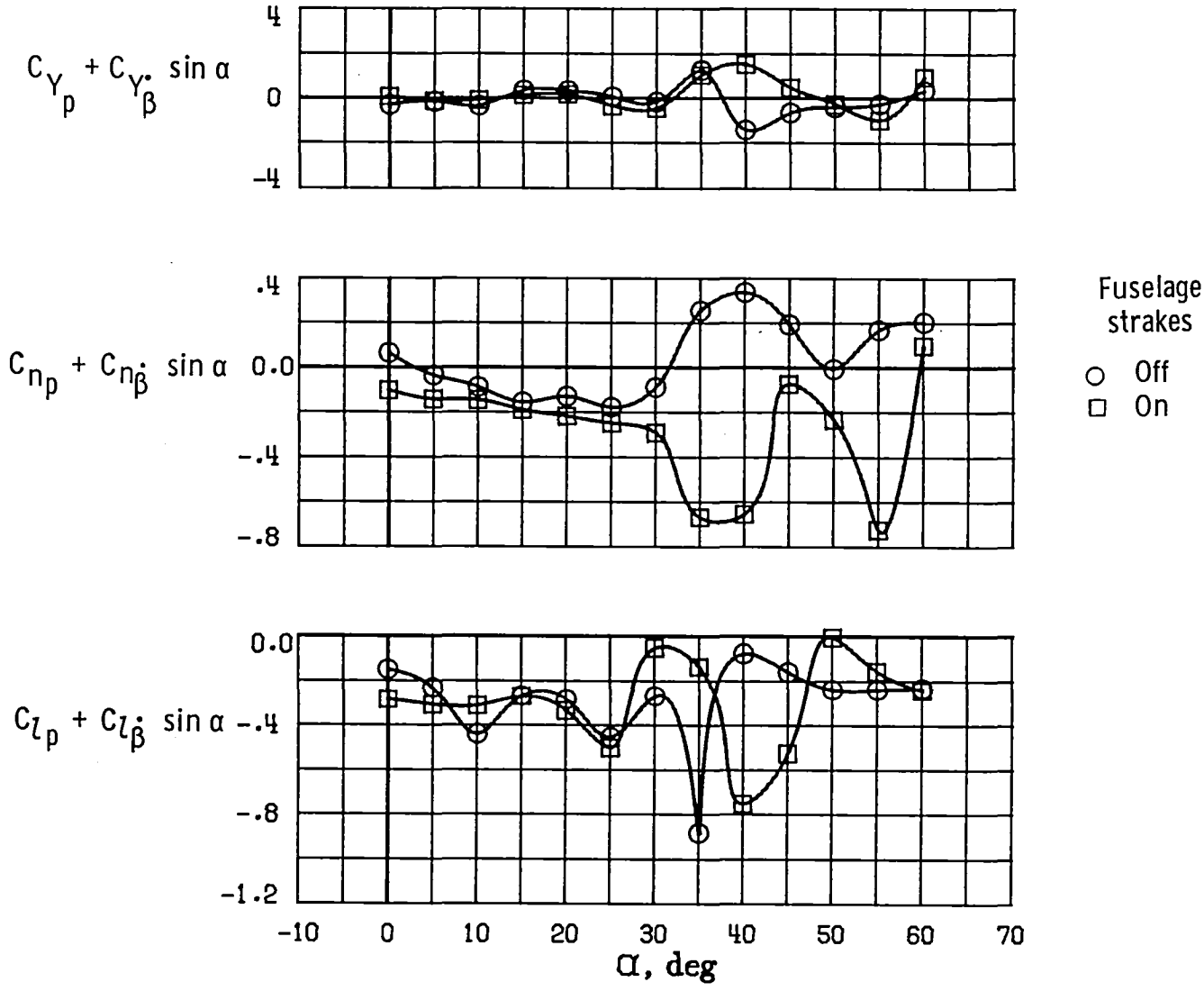

Figure 30.- Effect of fuselage strakes on dynamic rolling derivatives. $\Delta\theta = \pm 5°$; $\delta_c = 0°$; $k = 0.15$; $\delta_h = 0°$.

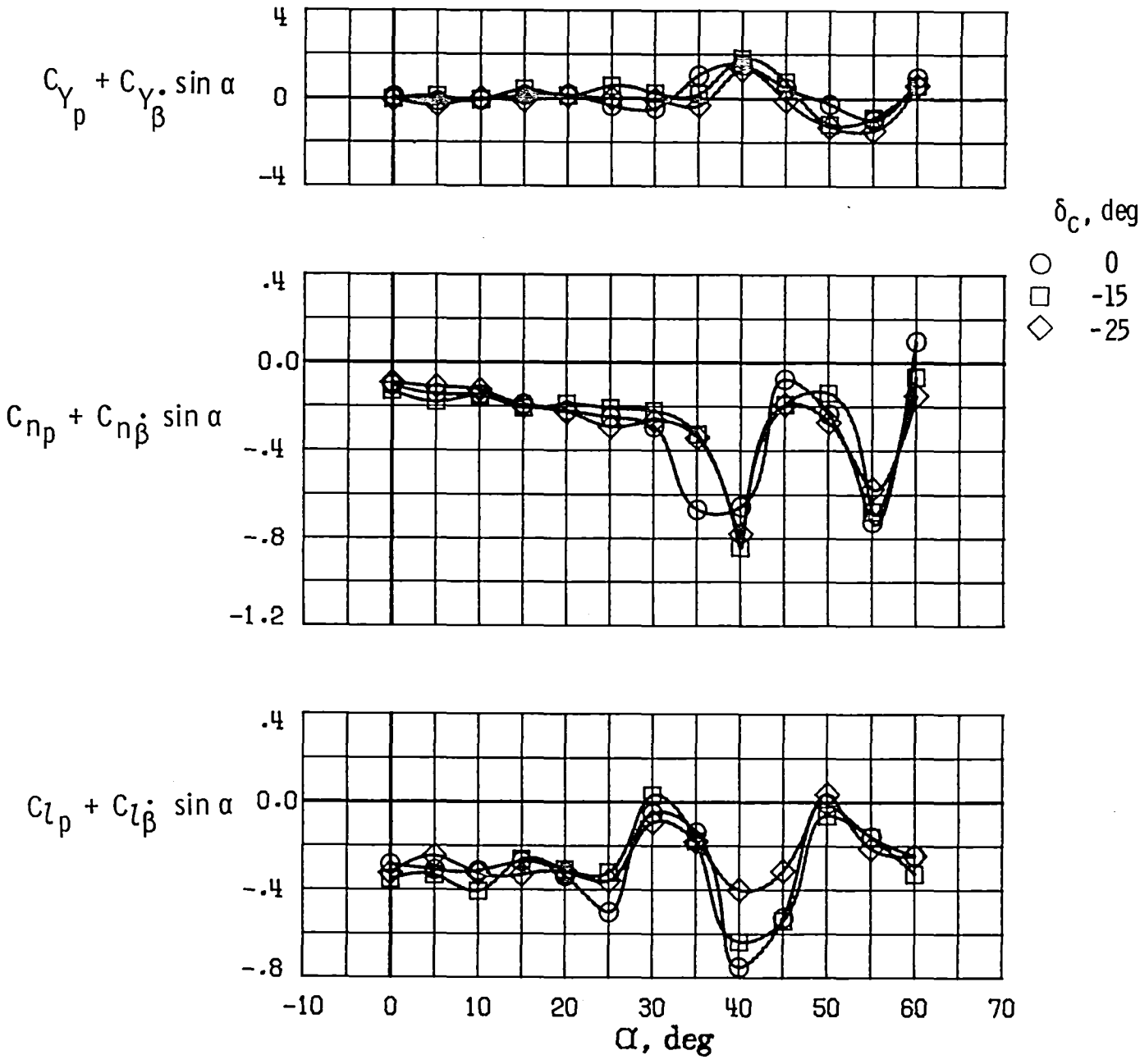

Figure 31.- Effect of canard deflections on dynamic rolling derivatives for the fuselage strakes. $\Delta\phi = \pm 5°$; $k = 0.15$; $\delta_h = 0°$.

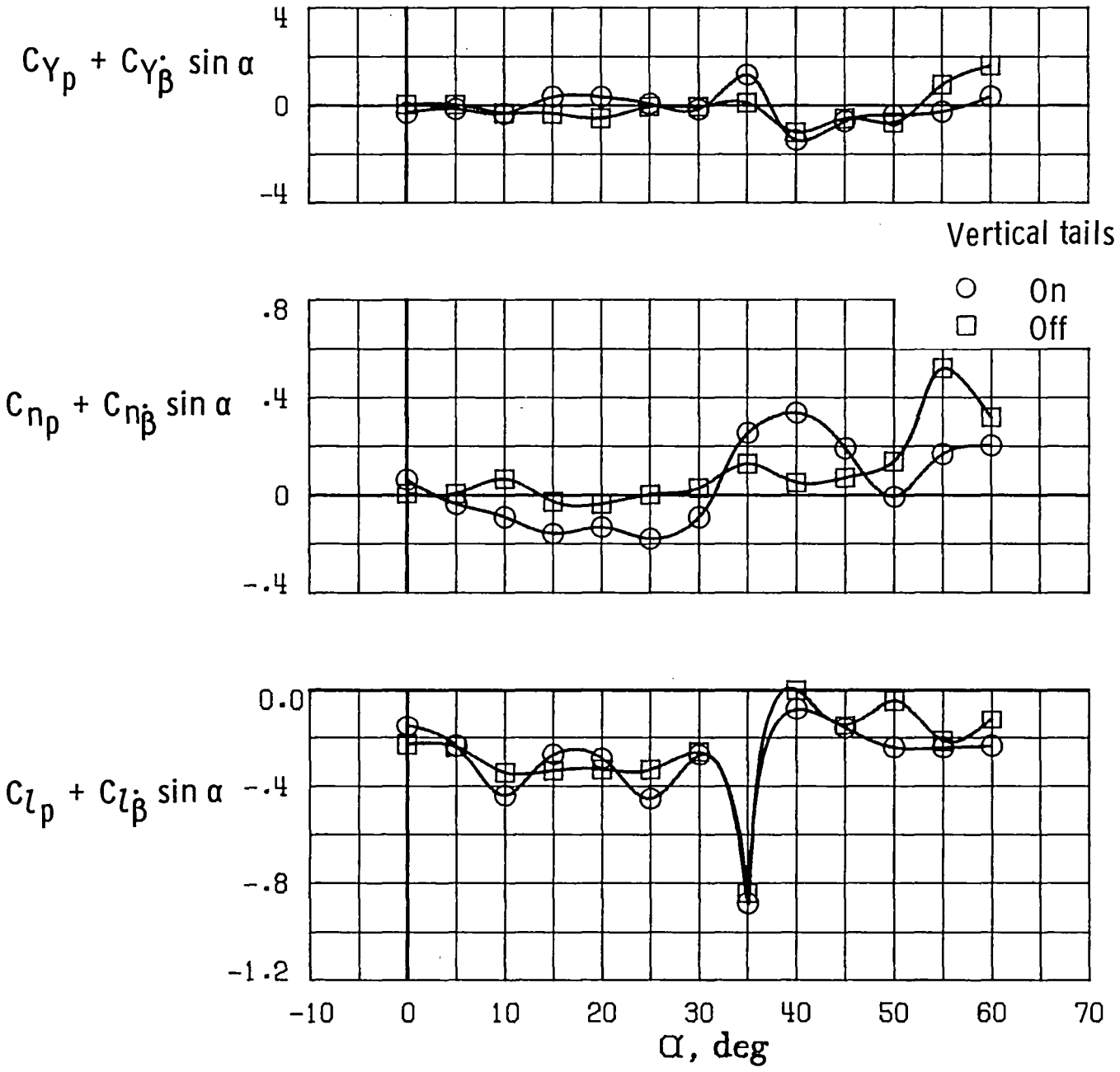

Figure 32.- Effect of vertical tails on dynamic rolling derivatives. $\Delta\phi = \pm 5°$; $\delta_c = 0°$; $\delta_h = 0°$; $k = 0.15$.

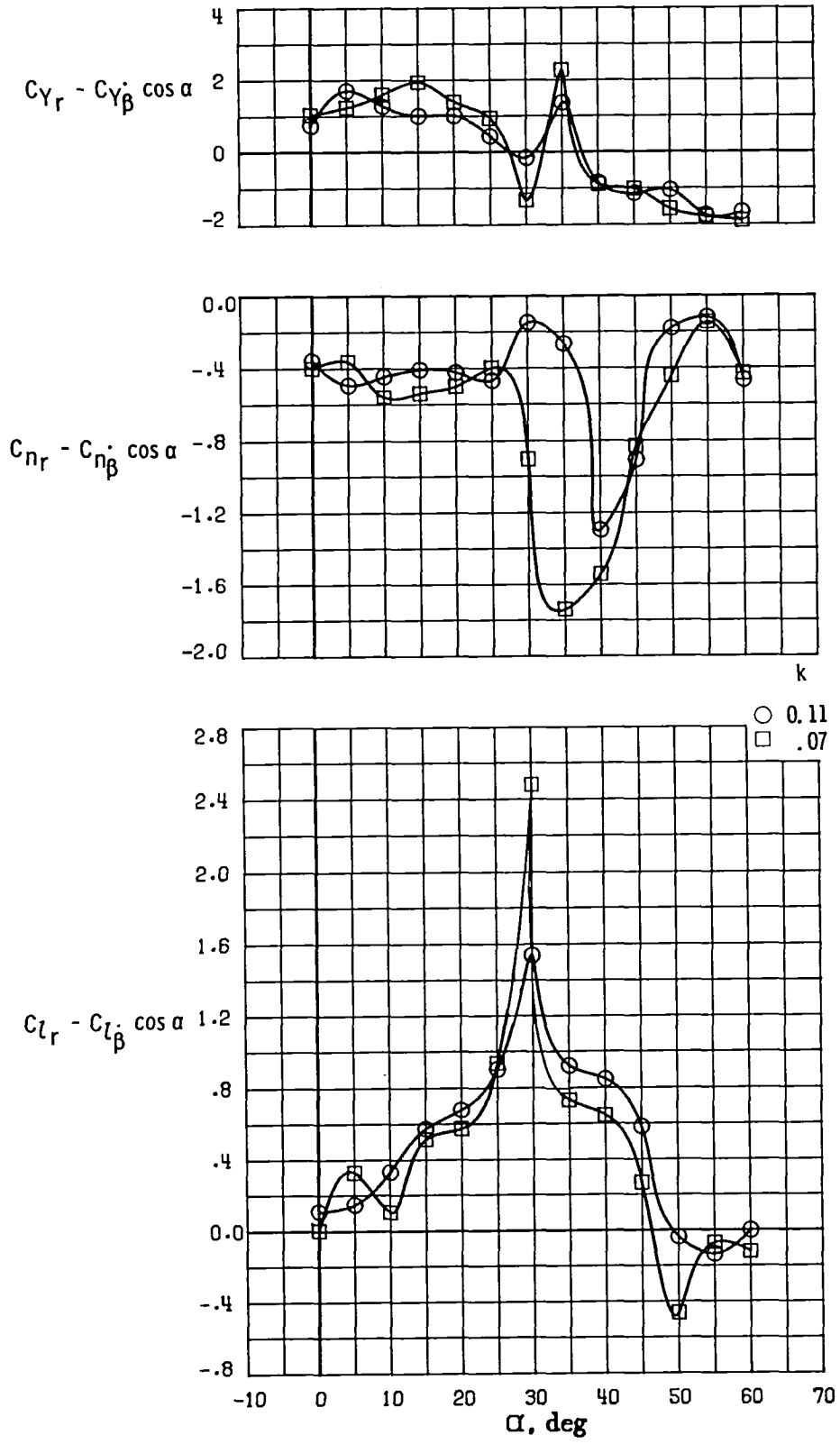

Figure 33.- Effect of frequency on dynamic yawing derivatives.
$\delta_c = 0°$; $\Delta\phi = \pm 5°$; $\delta_h = 0°$.

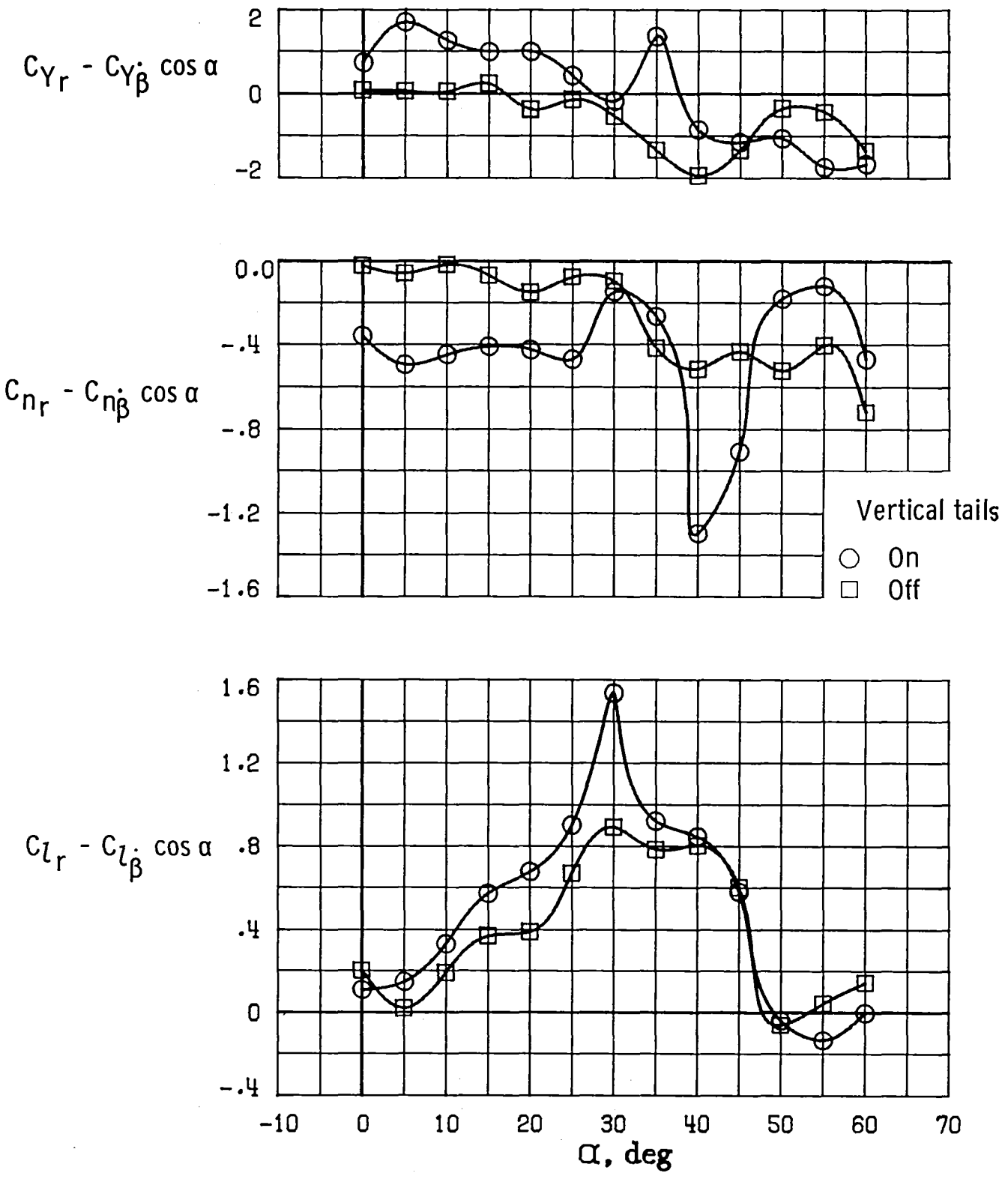

Figure 34.- Effect of vertical tails on dynamic yawing derivatives. $\delta_c = 0°$; $k = 0.11$; $\Delta\psi = \pm 5°$; $\delta_h = 0°$.

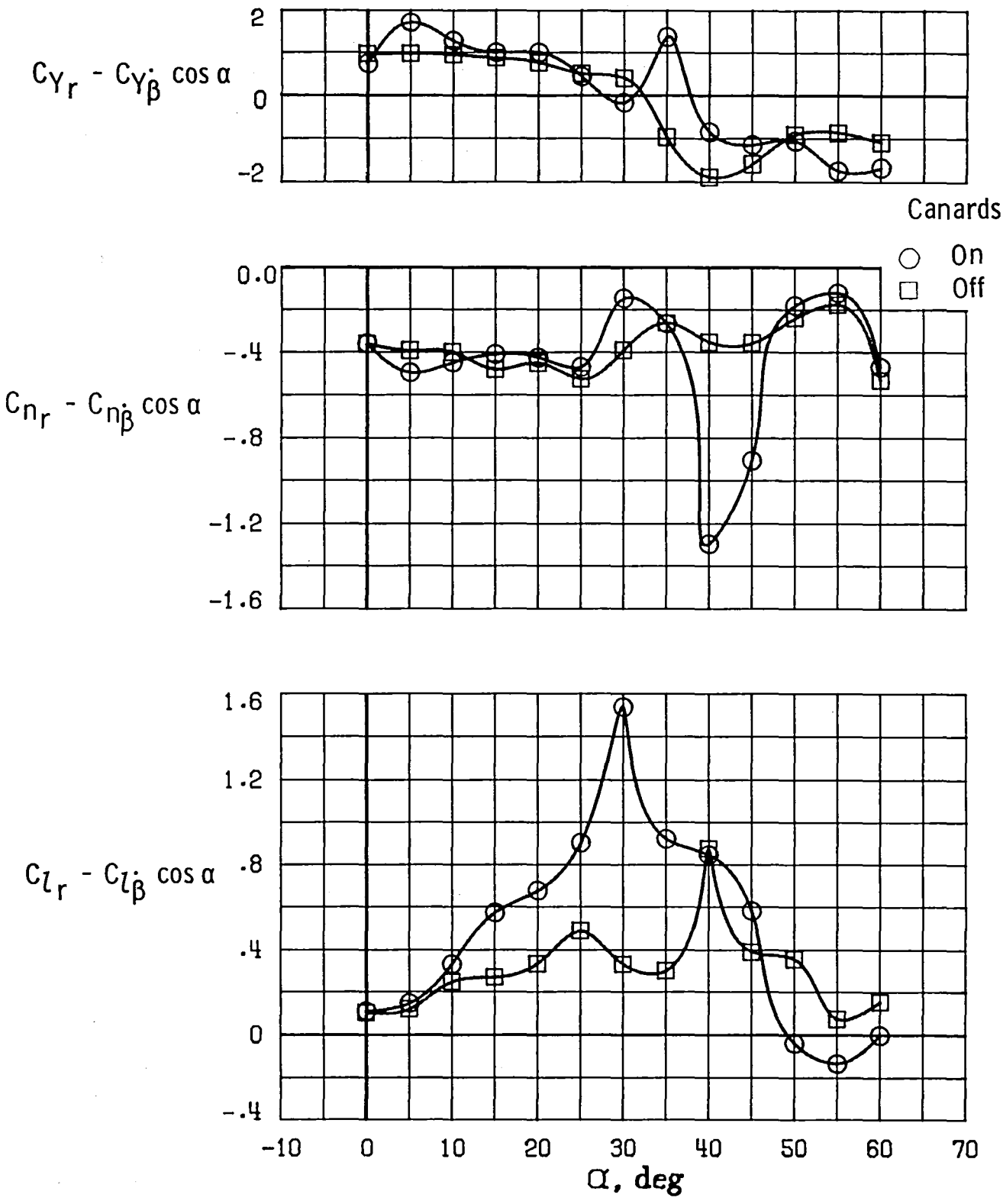

Figure 35.- Effect of canards on dynamic yawing derivatives. $\delta_c = 0°$; $k = 0.11$; $\Delta\psi = \pm 5°$; $\delta_h = 0°$.

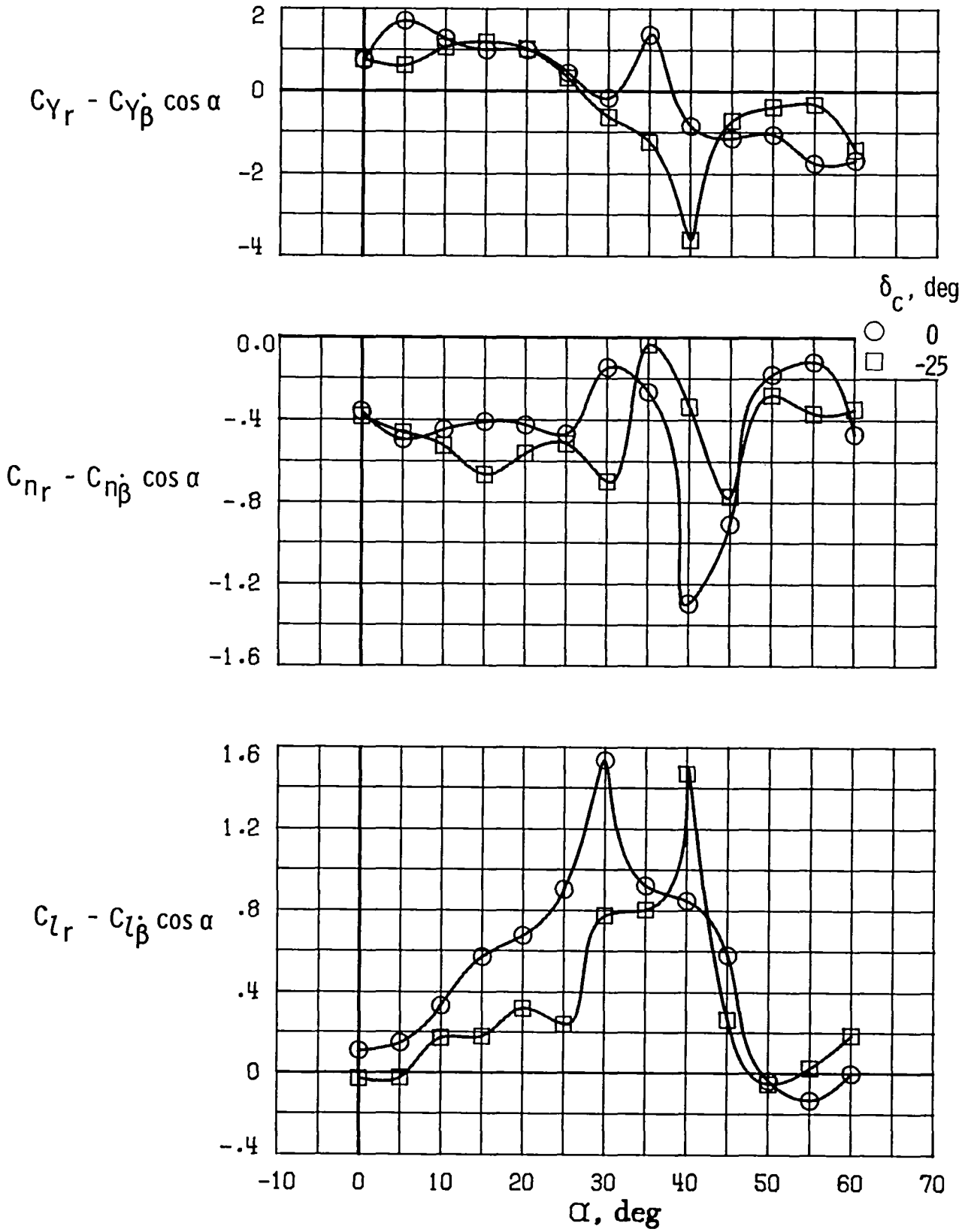

Figure 36.- Effect of canard deflection on dynamic yawing derivatives. $k = 0.11$; $\Delta\psi = \pm 5°$; $\delta_h = 0°$.

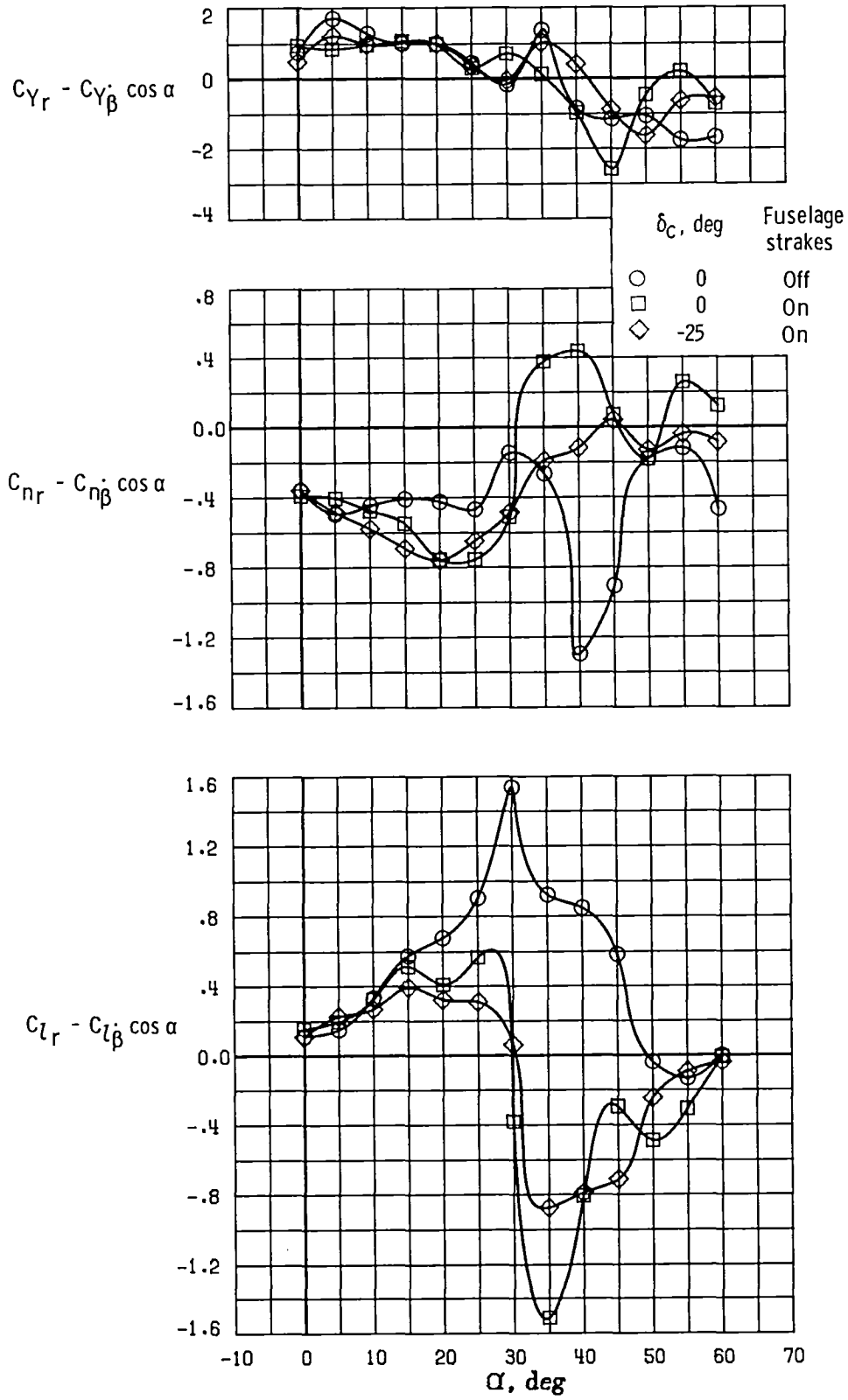

Figure 37.- Effect of fuselage strakes and canard deflection on dynamic yawing derivatives. k = 0.11; $\Delta\psi = \pm 5°$; $\delta_h = 0°$.

1. Report No.	2. Government Accession No.	3. Recipient's Catalog No.
NASA TM-84584		

4. Title and Subtitle	5. Report Date
HIGH-ANGLE-OF-ATTACK STABILITY CHARACTERISTICS OF A THREE-SURFACE FIGHTER CONFIGURATION	March 1983
	6. Performing Organization Code: 505-43-13-01
7. Author(s): Sue B. Grafton, Mark A. Croom, and Luat T. Nguyen	8. Performing Organization Report No.: L-15551
	10. Work Unit No.
9. Performing Organization Name and Address: NASA Langley Research Center, Hampton, VA 23665	11. Contract or Grant No.
	13. Type of Report and Period Covered: Technical Memorandum
12. Sponsoring Agency Name and Address: National Aeronautics and Space Administration, Washington, DC 20546	14. Sponsoring Agency Code

15. Supplementary Notes

16. Abstract

A wind-tunnel investigation was conducted to study the low-speed, high-angle-of-attack stability characteristics of a three-surface fighter concept based on the F-15 configuration. Static-force data were measured over angle-of-attack and side-slip ranges of 0° to 85° and -10° and 10°, respectively. A forced-oscillation technique was used to obtain dynamic derivatives at angles of attack from 0° to 60°. The tests were conducted for several canard deflections and with the canards removed to investigate the effects of the close-coupled canard on the high-angle-of-attack stability characteristics of the configuration. A fuselage strake was developed which significantly improved static lateral-directional stability characteristics at high angles of attack while also increasing the maximum lift of the configuration.

17. Key Words (Suggested by Author(s))	18. Distribution Statement
Stability Canards Three surface Dynamic Static Longitudinal Lateral directional	Unclassified - Unlimited Subject Category 08

19. Security Classif. (of this report)	20. Security Classif. (of this page)	21. No. of Pages	22. Price
Unclassified	Unclassified	58	A04

For sale by the National Technical Information Service, Springfield, Virginia 22161

NASA-Langley, 1983

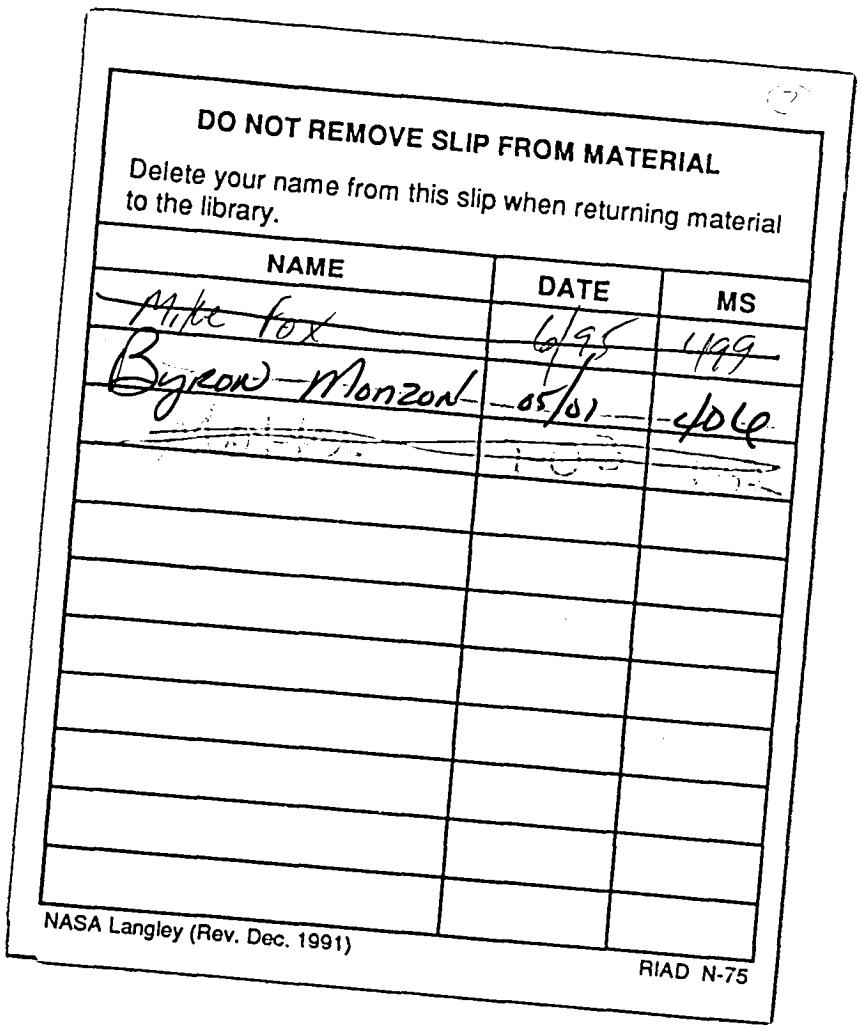

DO NOT REMOVE SLIP FROM MATERIAL

Delete your name from this slip when returning material to the library.

NAME	DATE	MS
Mike Fox	6/95	499
Byron Monzon	05/01	406

NASA Langley (Rev. Dec. 1991) RIAD N-75